Chapter 4

To develop and characterize starch-polyphenol complex from *Euryale ferox* seed

4.1 Introduction

The increasing incidence of obesity and type-2 diabetes mellitus across the globe have been linked to high-calorie dietary habits and sedentary lifestyles [9]. Although raw starches contain an appreciable amount of resistant starch, however, they are boiled before consumption, making them readily digestible, which is undesirable [11]. Foods with higher resistant starch (RS) proportion and lower glycemic index (GI) are beneficial for preventing obesity, insulin resistance, and diabetes owing to their potential to regulate post-prandial serum glucose levels and higher satiety value [7]. Polyphenols are extensively studied for its ability to inhibit starch digesting enzymes and are also regarded as a potential regulator for glucose uptake and metabolism [1]. We have witnessed a rise in interest in the usage of polyphenols to create starch-polyphenol complexes during the course of the last few years, which is an intriguing strategy to combat the current problems of diabetes and obesity [37]. *Euryale ferox*, an aquatic crop belonging to the *Nymphaeaceae* family which is generally cultivated for its edible seeds. The major component of the seed is starch, which makes up roughly 70% of the kernel. Whereas, the shell, which accounts for half of the seed, contains a substantial amount of polyphenols, but usually discarded. Epidemiological studies have shown that *Euryale ferox* seed shell extract could alleviate chronic ailments including type 2 diabetes, heart disease, and nephropathy because of its antioxidant, anti-hyperlipidemic, and anti-inflammatory properties. *Euryale ferox* seed shell contains gallic acid, catechin, ferulic acid, and rutin [31]. Polyphenols liberated from cellular compartments of seeds during processing could modified the physicochemical and functional properties of starch [7, 33, 16]. These compounds in the food ingredients are expected to interact during processing because of tissue rupture, mixing, and heating, ultimately affecting the colors, flavors, textures, and digestibility of *Euryale ferox* kernel starch.

The effects of tea polyphenols [17, 42], flavonoids from lotus leaf [35] on the characteristics of starch have been documented. The addition of gallic acid [4,5,13,24], ferulic acid [9, 16], quercetin [10, 20, 21, 25, 30, 33, 34,38,41,44], rutin [21, 33, 34], on the properties of maize starch, potato starch, rice starch, tartary buckwheat starch, wheat starch, cassava starch, lotus seed starch by employing hydrothermal treatment [20,21], high-pressure homogenization [42], and mechanical activation method [9], etc. have been evaluated. Nevertheless, pre-gelatinization and non-thermal techniques are frequently the

exceptionally widely employed techniques in starch-polyphenols complexation [37]. The pre-gelatinization process of complexation is the same as cooking; hence, it is safe and sustainable.

When starch is gelatinized, it releases amylose, rendering a proper environment for complexation. If polyphenols are introduced in this condition, polyphenols tend to dissolve and interact with the starch. Amylopectin is less likely to form complexes with polyphenols because the highly branched structure of amylopectin behaves as a steric hindrance [13, 35]. In most of cases, non-covalent bonds, especially hydrogen bonding, hydrophobic interactions, and van der Waals forces, are frequently accountable for attaching the hydroxyl group of polyphenols with starch molecules leading to the creation of inclusion or non-inclusion intermolecular aggregates. Starch-polyphenols complexes are less susceptible to starch digestive enzymes [10, 20, 21]. Furthermore, the starch-polyphenols complex exhibited the dual property of resistant starch along with the bioactivities of the attached polyphenol [7, 11].

Although the ultimate goal of starch modification with polyphenols is to lower starch digestibility and enhance the bio accessibility of polyphenols, the complexation unavoidably caused alterations to the characteristics of starch [37]. The characteristics of these complexes is determined by the type of starch, complexation method, type, and concentration of polyphenols [42]. Hence, the goal of the current study was to examine the effect of ferulic acid (FA) and quercetin (QR) on the structural, functional, and *in vitro* starch digestibility of *Euryale ferox* kernel starch. Studies have shown that a brief hydrothermal treatment did not have adverse effect on the functionality of polyphenols especially ferulic acid and quercetin [34, 37]. The study aims to fully understand the changes that might occur when *Euryale ferox* seed is boiled along with its shells. We hypothesized that during boiling, water soluble components may transfer from the shell into the starchy kernel. Further, this research also aims to develop a novel functional *Euryale ferox* kernel starch by combining it with polyphenols that may be used to produce lower glycemic index starch-based functional foods.

4.2 Materials and methods

4.2.1 Preparation of *Euryale ferox* kernel starch-polyphenols complex

The *Euryale ferox* kernel starch-polyphenols complex was produced by following the methods of Li et al. [20]. A slurry made up of 5 g of EFKS and 50 mL of distilled water was cooked at 90°C for 10 min while being vigorously shaken at 200 rpm. Then, polyphenols were added at the ratio of 2.5%, 5.0 %, 7.5 %, and 10.0 %, respectively to the starch. All the samples were agitated for another 1.5 h at 90°C. Pregelatinized starch (PS) was prepared according to the same procedure without polyphenols. The complex slurry obtained was divided into two parts: one portion was used for the *in vitro* starch digestibility experiment, and the other was allowed to cool before being dried, then crushed, and sieved through a 100 μm mesh. The samples were labelled as F1, F2, F3, and F4 indicating *Euryale ferox* kernel starch complexed with 2.5, 5, 7.5, and 10 g ferulic acid per 100 g starch respectively; Q1, Q2, Q3, and Q4 indicated *Euryale ferox* kernel starch complexed with 2.5, 5, 7.5 and 10 g quercetin per 100 g starch, respectively; GA1, GA2, GA3, and GA4 indicated *Euryale ferox* kernel starch complexed with 2.5, 5, 7.5 and 10 g gallic acid per 100 g starch, respectively; RT1, RT2, RT3, and RT4 indicated *Euryale ferox* kernel starch complexed with 2.5, 5, 7.5 and 10 g rutin per 100 g starch, respectively; CT1, CT2, CT3, and CT4 indicated *Euryale ferox* kernel starch complexed with 2.5, 5, 7.5 and 10 g catechin per 100 g starch, respectively; ES1, ES2, ES3, and ES4 indicated *Euryale ferox* kernel starch complexed with 2.5, 5, 7.5 and 10 g *Euryale ferox* seed shell per 100 g starch, respectively.

4.2.2 Characterization of *Euryale ferox* kernel starch-polyphenols complex

4.2.2.1 X-ray diffraction (XRD) analysis

X-ray powder diffractometer (Bruker AXS, Bruker Corporation, Germany) equipped with nickel purified Cu Ka radiation was operated to examine the diffraction patterns. The working voltage and current were calibrated to 40 kV and 40 mA, respectively. The XRD diffractograms were obtained with a step magnitude of 0.02 over a scattering range of 5-50° of 2θ.

4.2.2.2 Fourier transform infrared spectroscopy (FT-IR) analysis

An FT-IR spectrometer (Perkin Elmer, Waltham, MA) was used to analyze the functional groups of starch and its complexes. Samples were combined with properly dehydrated potassium bromide and pressed into pellets. FT-IR spectra emerged in the wavenumber range of 4000–400 cm^{-1} and were gathered with a resolution of 4 cm^{-1} at room temperature.

4.2.2.3 ^{1}H NMR spectroscopy analysis

Starch, polyphenols, and starch-polyphenols complexes (5 mg) were dissolved in 0.5 mL of deuterated dimethyl sulfoxide (DMSO-d6) and shifted into 5-mm NMR tubes for proton nuclear magnetic resonance (^{1}H-NMR) spectroscopy scanning. The ^{1}H NMR amplitudes of samples were then recorded using an AVANCE-600 spectrometer (Bruker Inc., Karlsruhe, Germany) which was set to operate at 25 ℃ and 500 MHz [10].

4.2.2.4 DSC analysis

The thermal properties of starch, polyphenols, and starch-polyphenols complexes were examined operating a differential scanning calorimeter (DSC-60, Shimadzu, Tokyo, Japan). Samples (3mg) were closed in aluminum sample holder and scanned from 30 to 350 ℃ at a rate of 10 ℃/min. As a reference, an empty aluminum pan was utilized [33].

4.2.2.5 Scanning electron microscopy (SEM) analysis

The microscale three-dimensional form of the starch, and starch polyphenols complex granules were investigated operating a scanning electron microscope (JSM-6360LV, JEOL, Japan) function in a low vacuum system at a 10 kV accelerating voltage. Before the analysis, samples were placed onto a double-sided tape using specimen holder, then coated with gold in an ion coater to impart conductivity in a vacuum evaporator. SEM micrographs were taken at 500x magnification.

4.2.3 *In-vitro* starch digestibility

4.2.3.1 Determination of starch fractions

The *in vitro* digestibility of starch was evaluated following the methodology previously outlined by Englyst et al. (1997) [8]. Cooked samples were hydrolyzed by using enzyme mixture consisting of porcine pancreatin α-amylase (80U/mL) and amyloglucosidase

(1000 U/mL) in 10 mL sodium acetate buffer (pH 5.2). In order to hydrolyze the starch into glucose, the reaction mixture was incubated at 37 °C with moderate stirring in a water bath. An aliquot of 0.5 mL from each flask was withdrawn at each 20 min for 3 h, and the enzymes were immediately inactivated by adding 20 mL of 66 % ethanol. The aliquots were centrifuged at 3000 *g* for 10 min, and the release glucose was measured using a glucose oxidase peroxidase (GAGO-20) reagent. The amount of hydrolyzed starch was calculated by multiplying glucose content by 0.9. The total starch content of the samples was the mass of starch [6]. The amount of starch hydrolyzed at various time periods was used to express the rate of starch digestion. The following equations were used to determine the amounts of RDS, SDS and RS in the samples:

$$\text{RDS}\ (\%) = \frac{G_{20} - G_0 \times 0.9}{\text{TS}} \times 100 \quad (1)$$

$$\text{SDS}\ (\%) = \frac{(G_{120} - G_{20}) \times 0.9}{\text{TS}} \times 100 \quad (2)$$

$$\text{RS}(\%) = \frac{\text{TS} - (G_{120}) \times 0.9}{\text{TS}} \times 100 \quad (3)$$

TS was the weight of the sample (1g); whereas for the complexes, total starch was the weight of the samples excluding added polyphenols

4.2.3.2 Predicted glycemic index (pGI)

The rate of starch digestion was expressed as the percentage of total starch (TS) hydrolyzed at different times (20, 40, 60, 80, 100, 120, and 180 min). According to the equation of Goni et al. [12], the kinetics of starch hydrolysis were calculated using the first order equation: $C = C\infty\ (1 - e^{-kt})$, where C is the percentage of starch hydrolyzed at time t (min), $C\infty$ is the extent of maximum hydrolysis, k is kinetic constant, and t is time (min). The following equation was used to calculate the area under the hydrolysis curve (AUC):

$$\text{AUC} = C\infty\ (t_f - t_o) - (C\infty / k)\ [\ 1 - \exp^{\{-k\,(t_f - t_o)\}}]. \quad (4)$$

Where $C\infty$ is the percentage of starch hydrolyzed at 180 min, t_f is the final time (180 min), t_0 is the initial time (0 min) and k is the kinetic constant.

The ratio of AUC of each sample to the AUC of the control white bread was used to determine the hydrolysis index (HI). The HI value obtained for each sample was used in the equation given below for determining the pGI [12]:

$$\text{Hydrolysis Index} = \frac{\text{AUC of each sample}}{\text{AUC of reference white bread}} \times 100 \quad (5)$$

The formula pGI =39.71+0.549HI was used to determine the predicted glycemic index (pGI).

4.2.4 Determination DPPH free radical scavenging activity

The DPPH (2,2-diphenyl-1-picrylhydrazyl) free radical scavenging ability of each extract was assessed by following the method of Dudonne [9]. The change in absorbance at 515 nm was determined after incubating the samples in a water bath for 20 min at 37°C (A_E). Similarly, a blank sample containing 100 mL of methanol in place of EFSSE was added into the DPPH solution was prepared in the same way, and its absorbance was noted as A_B. The following formula was used to estimate the amount of free radical scavenging capacity:

$$\%\, inhibition = \frac{A_B - A_E}{A_B} \times 100 \quad (6)$$

where A_B: absorbance of the blank sample, and A_E: absorbance of the plant extract

4.2.5 Color properties

The color characteristics of *Euryale ferox* kernel starch was analyzed using a colorimeter (Ultrascan VIS, Hunterlab, USA). Results were reported in terms of Lightness (L*) values extend from 0 (black) to 100 (white). Positive a* represents redness and negative a* represents greenness while positive and negative b* represents yellowness and blueness respectively.

4.2.6 Swelling power and solubility index

The swelling power and solubility index of the complexes were evaluated by using the method explained by Karunaratne and Zhu (2016) [11] with slight modification. Briefly, samples of 100mg were mixed with 10 mL of water. The mixture was vortex for 2 min and incubated at 90 ℃ in a water bath for 30 min. Then, the tubes were brought to room

temperature, and centrifuged at 2000g for 30 min and the weight of the sediment was recorded, while the supernatants thus obtained was carefully collected into a pre-weighed aluminum can, and kept in a hot air oven at 105 °C until the weight remain constant and their difference was the weight of the dried supernatant. The following equations were used to determine the solubility index and swelling capacity.

$$\text{Swelling power (g/g)} = \frac{W_1}{W} \tag{7}$$

$$Solubility\ (\%) = \frac{W_2}{W} \times 100 \tag{8}$$

where, W, W1, and W2 represents the weight (g) of sample, wet sediments, and dried supernatants respectively.

4.2.7 Statistical analysis

Three repetitions of each experiment were carried out. The experimental results were subjected to analysis of variance (ANOVA). Significant differences between the data were obtained by Tukey's tests using SPSS 24 (IBM Analytics, USA) and p value < 0.05 was considered statistically significant.

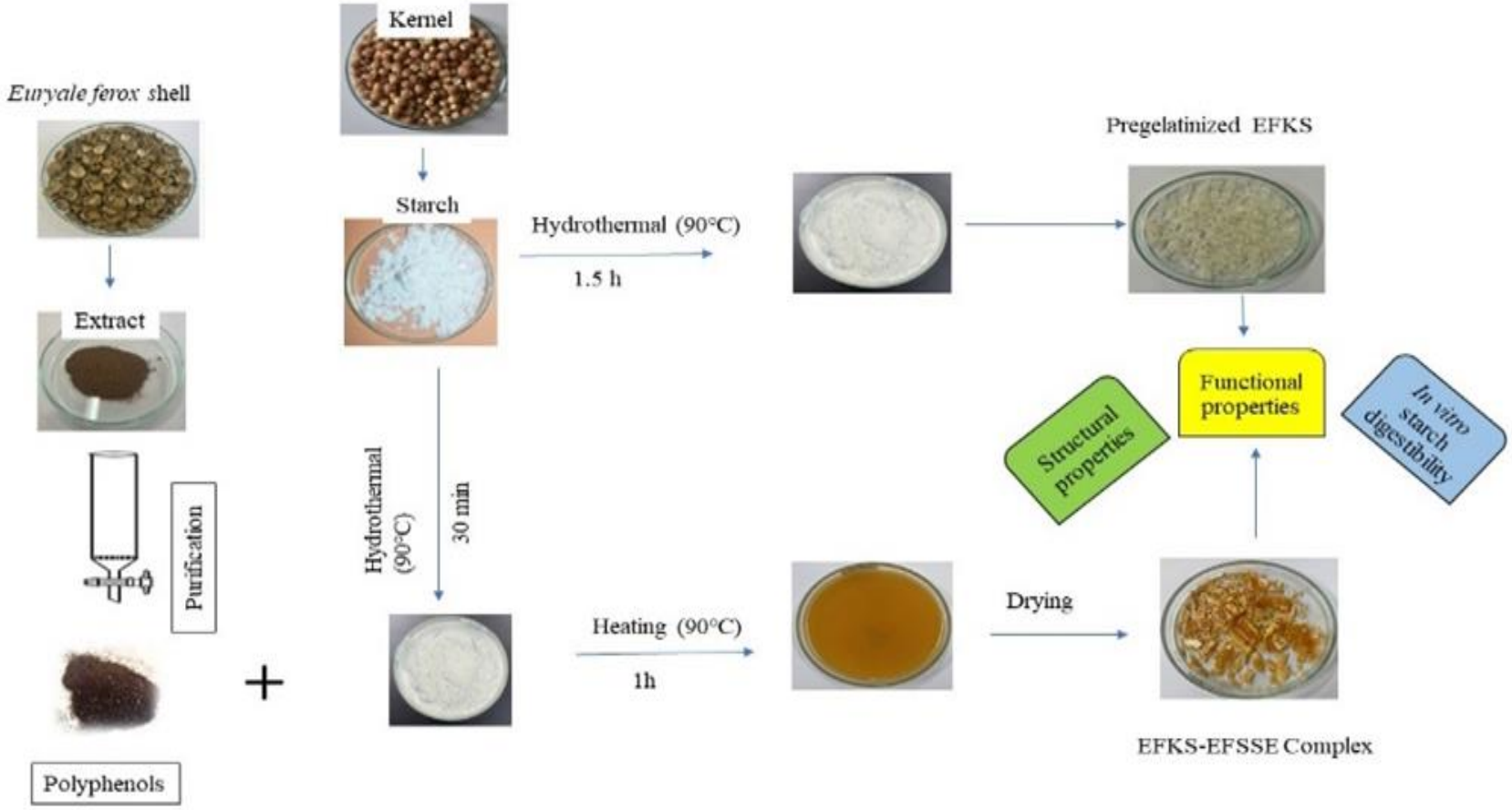

Fig. 4.1 Preparation and characterization of *Euryale ferox* kernel starch-polyphenol complex

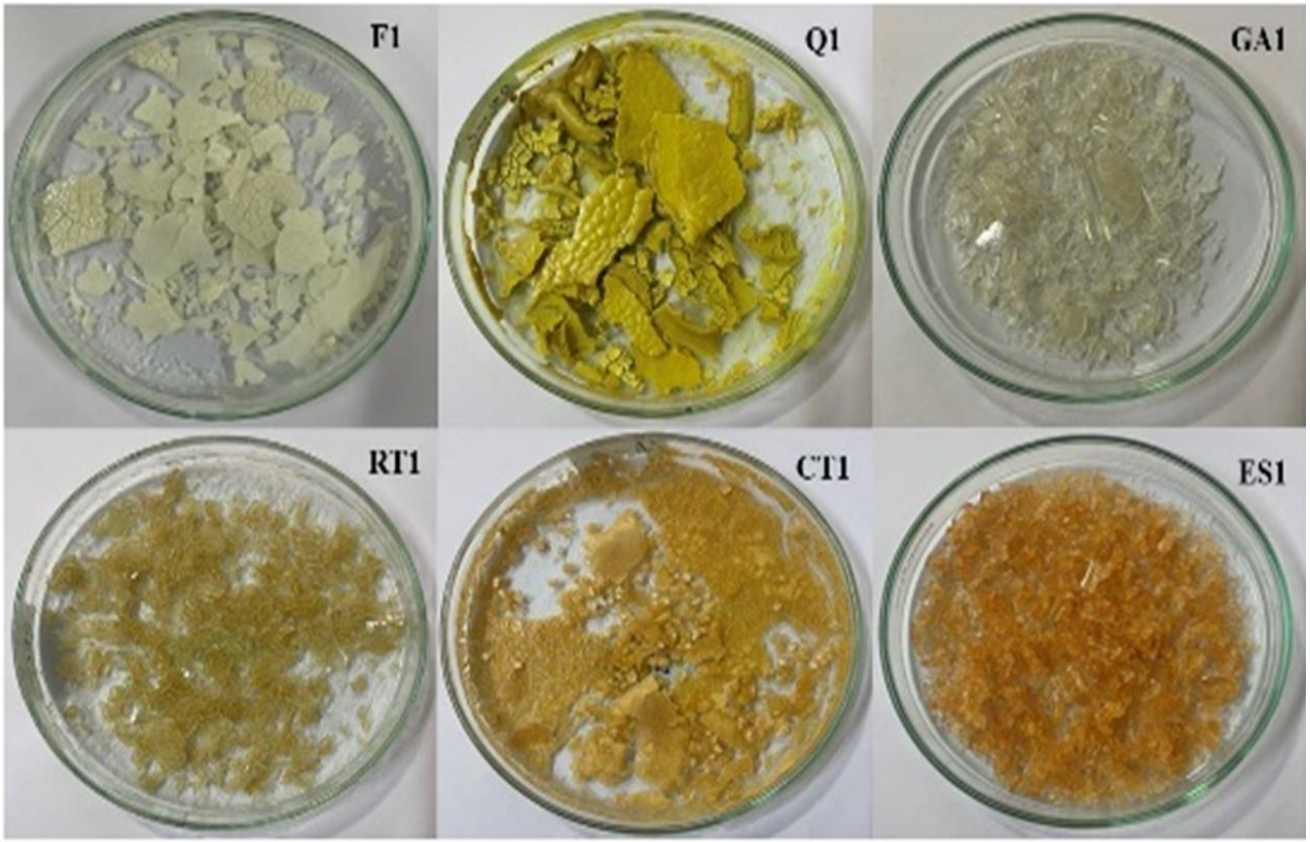

Fig. 4.2 (F1) *Euryale ferox* kernel starch-ferulic acid complex; **(Q1)** *Euryale ferox* kernel starch-quercetin complex; **(GA1)** *Euryale ferox* kernel starch-gallic acid complex; **(RT1)** *Euryale ferox* kernel starch-rutin complex; **(CT1)** *Euryale ferox* kernel starch-catechin complex; **(ES1)** *Euryale ferox* kernel Starch- *Euryale ferox* seed shell extract complex

4.3 Results and discussion

4.3.1 Characterization of *Euryale ferox* kernel starch-polyphenols complex

4.3.1.1 X-ray diffraction (XRD)

The impact of polyphenols on the crystalline structure of EFKS was assessed and the XRD spectra of the samples are displayed in Fig. 4.3. The native *Euryale ferox* kernel starch exhibited A-type XRD patterns having diffraction peaks at 15 and 23° and a twined peak at 17 and 18° [40]. The pre-gelatinized *Euryale ferox* kernel starch (PS) exhibited an amorphous diffraction pattern, indicating that gelatinization had completely destroyed the crystallinity of the starch granules [13].

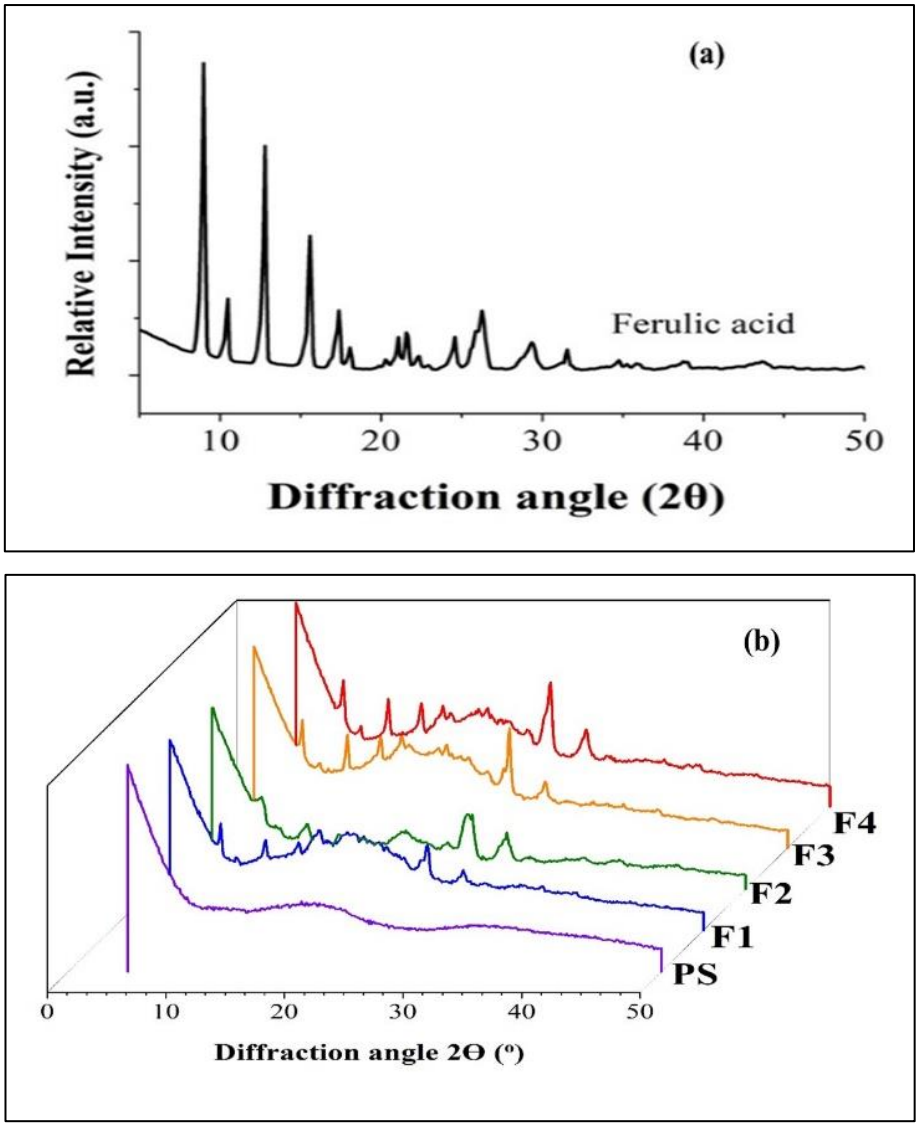

Fig. 4.3 (a) XRD pattern of ferulic acid; **(b)** XRD pattern of *Euryale ferox* kernel starch-ferulic acid complex

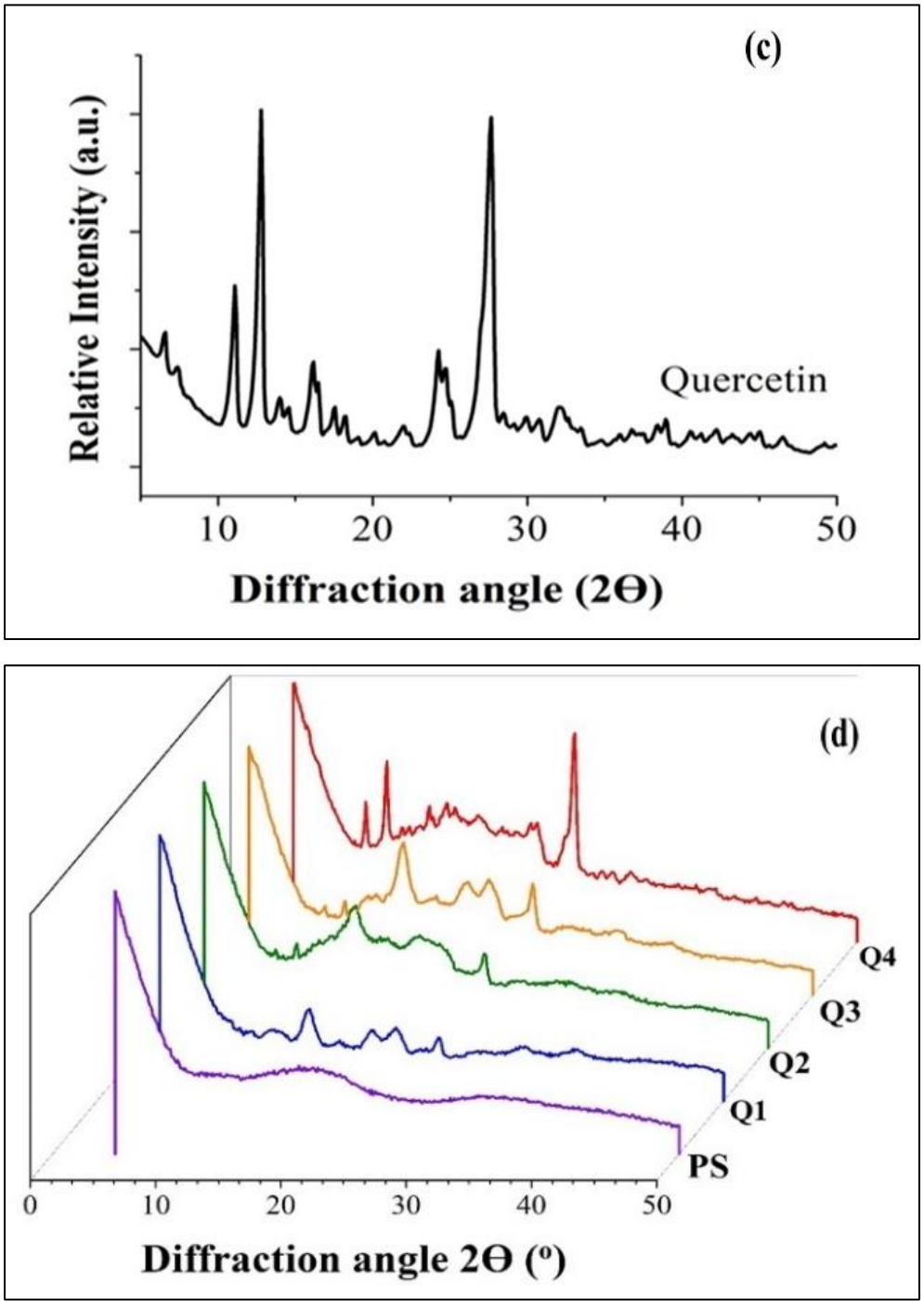

Fig. 4.3 (c) XRD pattern of quercetin; **(d)** XRD pattern of *Euryale ferox* kernel starch-quercetin complex

The diffraction pattern of pure ferulic acid [Fig. 4.3 (a)] revealed its crystalline nature having diffraction peak at 8.99, 10.48, 12.78, 15.58, 17.37, 18.07, 20.27, 21.06, 21.56, 22.36, 24.56, 25.86, 26.26, 29.35 and 31.55° of 2θ. In contrast to the control starch, increased in crystallinity in the complexes, indicated by sharper peaks migrated from ferulic acid, particularly those at 9.09, 12.98, 15.68, 17.57, 20.67, 21.67, 26.26, 29.35 and 31.55° of 2θ as well as multiple less prominent peaks was found in the EFKS-ferulic acid complex [Fig. 4.3 (b)]. Further, the intensity of the distinctive peak at 26.26 and 29.35° of 2θ found in the developed complexes increased as the amount of ferulic acid increased. The hydroxyl groups in the starch chains formed complexes with the hydrolyze ferulic groups, which disrupted some of the intermolecular hydrogen bonds and altered the crystal structure. Similar outcomes have been demonstrated in starch-ferulates produced through mechanical activation, where ferulates were encased inside the hydrophobic area of the double helices of the linear chain amylose molecules and developed cassava starch-ferulic acid complex [9].

Pure quercetin [Fig. 4.3 (c)]. has multiple distinct peaks in its diffraction pattern, specifically at 6.59, 7.39, 11.08, 12.78, 13.98, 14.58, 16.17, 16.47, 17.57, 18.27, 18.97, 20.17, 21.96, 24.26, 27.65, 29.95, 32.04 and 38.93^{o} of 2θ indicating its crystalline nature. It was observed that some of the prominent peaks of quercetin specifically at 10.38, 12.88, 13.98, 14.78,15.77, 16.77, 18.67, 18.97, 19.27, 21.86, 22.56, 22.86, 23.76, and 27.25° of 2θ were present in the EFKS-quercetin complex [Fig. 4.3 (d)]. The interaction of quercetin with *Euryale ferox* kernel starch, could produce a relatively well-organized crystalline structure. Furthermore, the intensity of the distinctive peak at 27.65° in the complexes increased as the amount of quercetin increased because the hydroxyl groups of polyphenols may bind to the starch chains and behave as a plasticizer or cross-linker to strengthen the molecular arrangement [5]. These intra and intermolecular hydrogen bonding within the starch and starch polyphenols molecules would be responsible for the crystalline structures of the complexes; causing amorphous area to become more organized and crystalline area to become tighter [17]. However, the intensity of the specific diffraction peak of quercetin at 27.65° was comparatively lesser as compare to the pure quercetin, indicating that in spite of quercetin implanted into starch granules, because the shift in inter- or intramolecular hydrogen bonds was insufficient to modify the crystal structure [20].

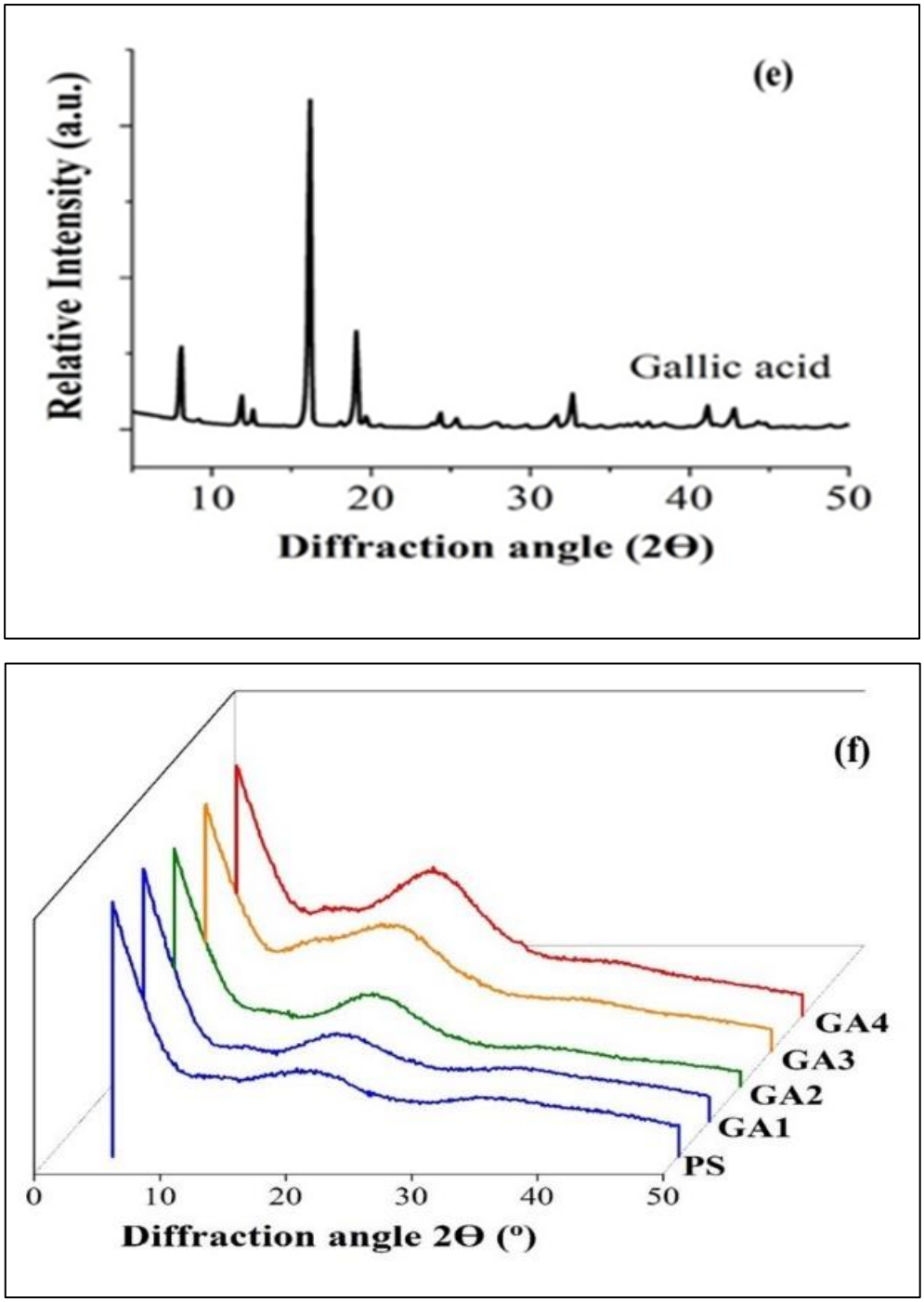

Fig. 4.3 (e) XRD pattern of gallic acid; **(f)** XRD pattern of *Euryale ferox* kernel starch-gallic acid complex

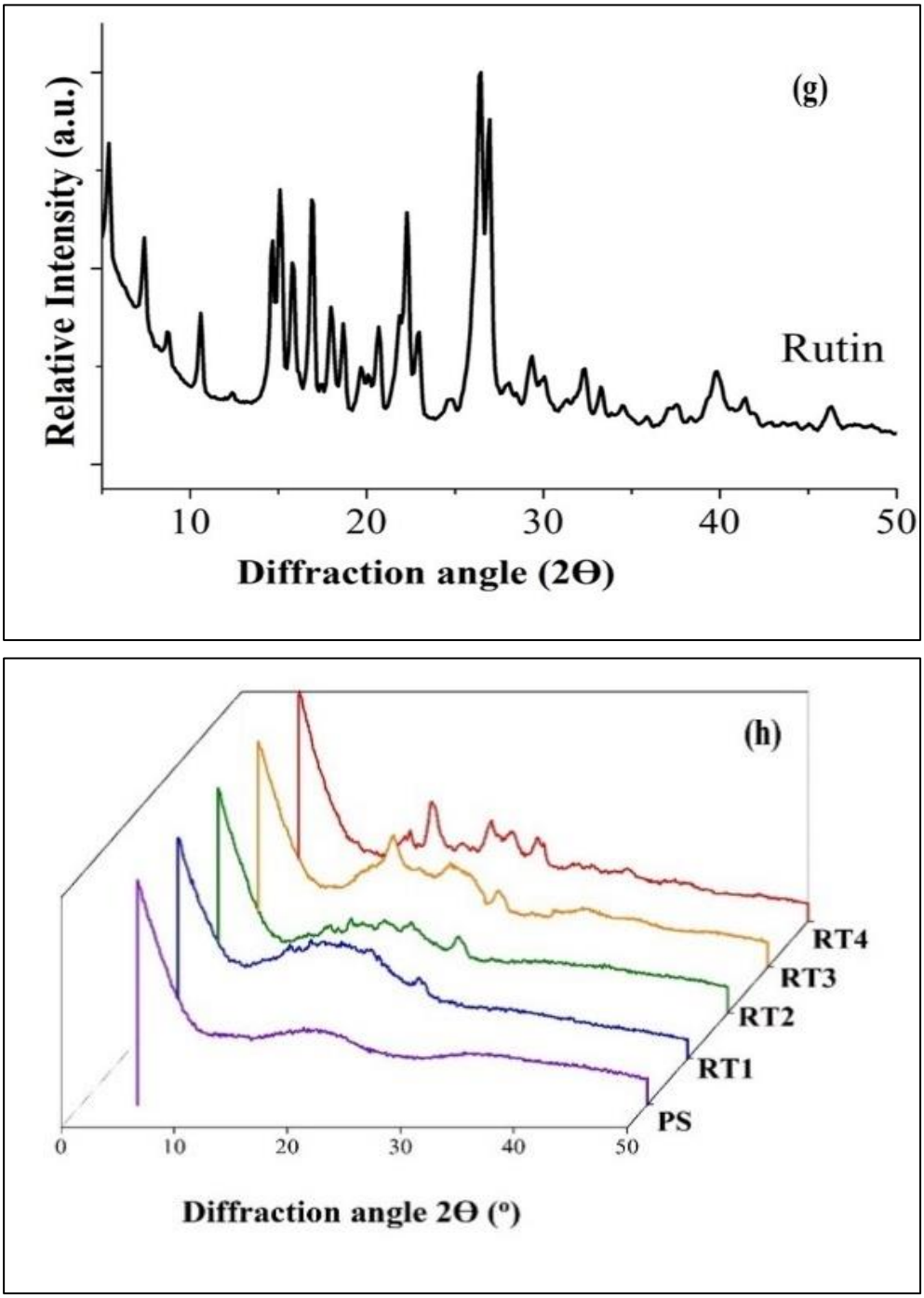

Fig. 4.3 (g) XRD pattern of rutin; **(h)** XRD pattern of *Euryale ferox* kernel starch-rutin complex

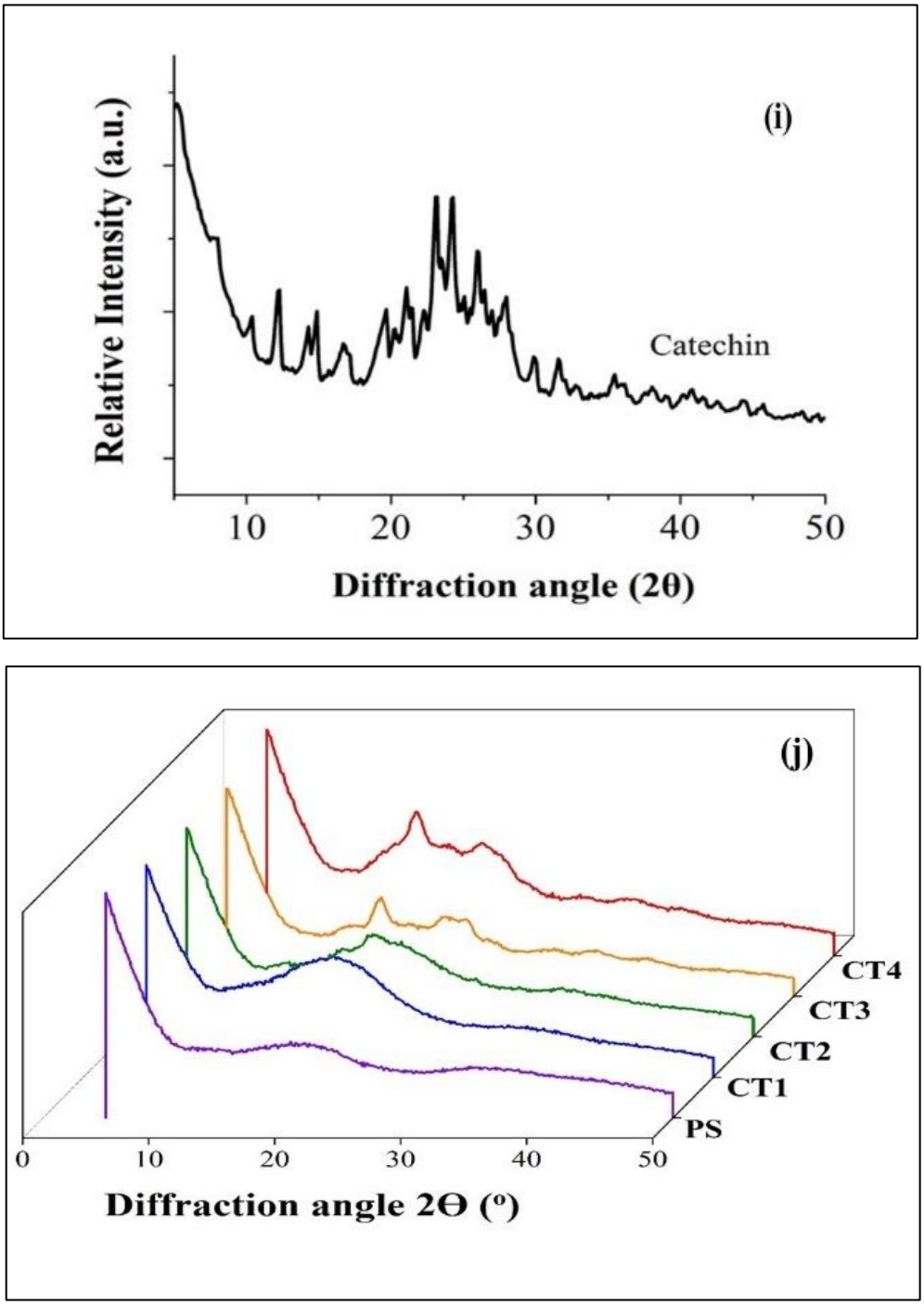

Fig. 4.3 (i) XRD pattern of catechin; **(j)** XRD pattern of *Euryale ferox* kernel starch-catechin complex

Pure gallic acid has multiple distinct peaks in its diffraction pattern, specifically at 8.09, 16.17, and 19.036^{o} of 2θ indicating that its crystalline nature. Minor peaks at 11.85, 12.66, 24.32, 25.29, 31.56, 32.62 were also present [Fig. 4.3 (e)]. However, unlike the quercetin and ferulic acid complexes, EFKS-gallic acid complexes did not show any characteristics

peak of gallic acid, there was only one broad peak at around 20^{o} of 2θ [Fig. 4.3 (f)]. The typical peaks of gallic acid in EFKS-gallic acid disappeared after complexation, demonstrating that specific molecular arrangement of starch and gallic acid created a typical V-type helical structure by intermolecular rearrangement of orders, evading the particular diffraction peak of gallic acid. However, the inclusion of gallic acid increased the crystallinity of EFKS-gallic acid.

A strong and clear diffraction peaks of pure rutin specifically at 5.39, 7.39, 8.69, 10.58, 14.68, 15.08, 15.77, 16.87, 17.97, 18.67, 19.67, 20.67, 22.26, 22.96, 26.45, 26.95, 29.35, 32.34 and 39.83^{o} of 2θ indicating its crystalline nature [Fig. 4.3 (g)]. The XRD patterns of the complexes hardly showed any signs of the original rutin characteristic peaks. However, it was observed that some of the prominent peaks of rutin specifically at 14.88, 16.77, 22.06, 23.86, and 26.06 ° of 2θ were found to be present in the spectra of the EFKS-rutin complexes in a very low intensity [Fig. 4.3 (h)]. Further, the intensity of the distinctive peak at 16.77 and 26.06° of 2θ found in the developed complexes increased as the amount of rutin increased. It was anticipated that it would have improved solubility and bioavailability under such circumstances.

Pure catechin has multiple distinct peaks in its diffraction pattern, specifically at 7.69, 7.99, 10.38, 11.08, 11.48, 12.28, 14.28, 14.88, 16.67, 19.67, 20.27, 21.06, 22.26, 23.16, 23.46, 24.26, 25.06, 25.96, 26.45, 27.95, 29.85, and 31.55^{o} of 2θ indicating its crystalline nature [Fig. 4.3 (i)]. It was observed that some of the peaks of catechin specifically at 16.85 and 22.53 of 2θ were found to be present in the spectra of EFKS-catechin complexes [Fig. 4.3 (j)]. Although, the intensity of these distinctive peak found in the developed complexes was remarkably low as compared to the pure compounds, yet the crystallinity increased of the complexes as the amount of catechin increased.

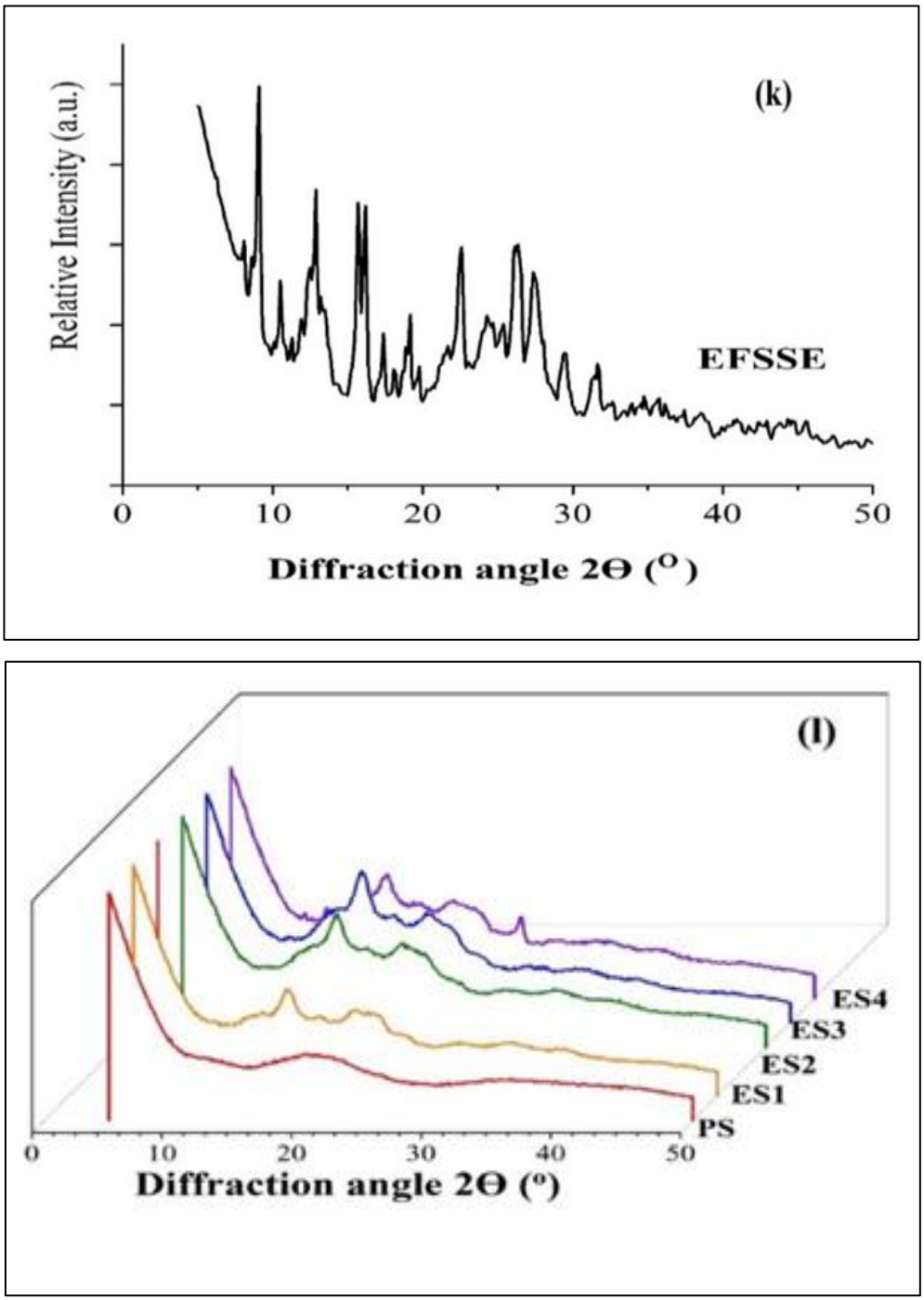

Fig. 4.3 (k) XRD pattern of *Euryale ferox* seed shell extract; **(l)** XRD pattern of *Euryale ferox* kernel starch-*Euryale ferox* seed shell extract complex

In case of starch-polyphenols complex prepared by adding *Euryale ferox* seed shell extract, it was observed that some of the peaks of polyphenols specifically at 26.85 and 32.53 of 2θ from EFSSE [Fig. 4.3 (k)] were found to be present in the spectra of the EFKS-EFSSE

complexes [Fig. 4.3 (l)]. Further, the intensity of these distinctive peak found in the developed complexes increased as the amount of EFSSE increased.

In the present study, starch-polyphenols complexation produced a new structure that was different from the V-type pattern. It is because, starch and polyphenols must interact in the presence of an organic solvent, an acid, or an alkali for a sufficiently long period of time to induce V-type inclusion complexation [1, 14, 20]. However, the complexation methods employed in the present study was modest and are bound to happen during food processing [22]. It was reported that ferulic acid, quercetin, or tannins could not form V-type inclusion complexes, because the size of these polyphenols is too large and prevented from reaching the cavity of amylose and hence amylose could not enclose the polyphenols [29]. Some of the earlier studies have demonstrated that the complexation between starch molecules and polyphenols was mostly driven by hydrophobic interactions [10].

4.3.1.2 Fourier transform infrared (FT-IR) spectroscopy

The FTIR spectrum of ferulic acid [Fig. 4.4 (a)] displayed its characteristics absorption peaks at 3436 cm^{-1} (O-H), 3021 cm^{-1} (C-H stretching), 1754 cm^{-1} (C=O stretching), and 1513 cm^{-1} and 1637 cm^{-1} (C=C bonds). Two small and sharp peaks at 803 cm^{-1} and 852 cm^{-1} attributed to hydrogen atoms on the phenyl ring of ferulic acid. On the other hand, the characteristics band of starch were present at 3372 cm^{-1} because of O-H stretching, and 1018-1083 cm^{-1} associated with pyranose ring of glucose. Some other bands at 1648, 1458, 1159,1009, 923, 848, 755 cm^{-1} were also observed [Fig. 4.4 (b)]. The characteristic peaks of both ferulic acid and starch were present on the *Euryale ferox* kernel starch-ferulic acid complexes [Fig. 4.4 (b)].

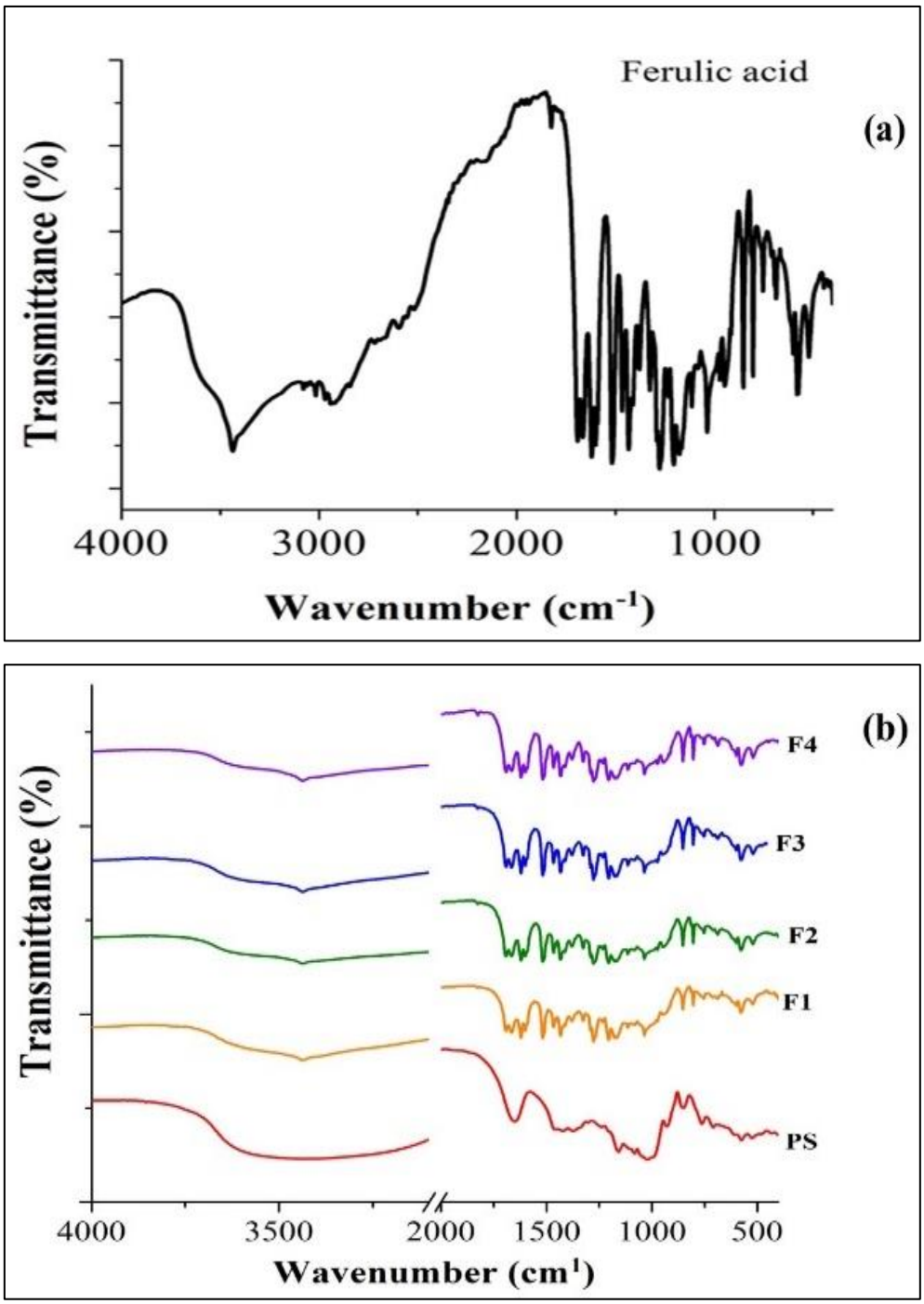

Fig. 4.4 (a) FTIR spectra of ferulic acid; **(b)** FTIR spectra of *Euryale ferox* kernel starch-ferulic acid complex

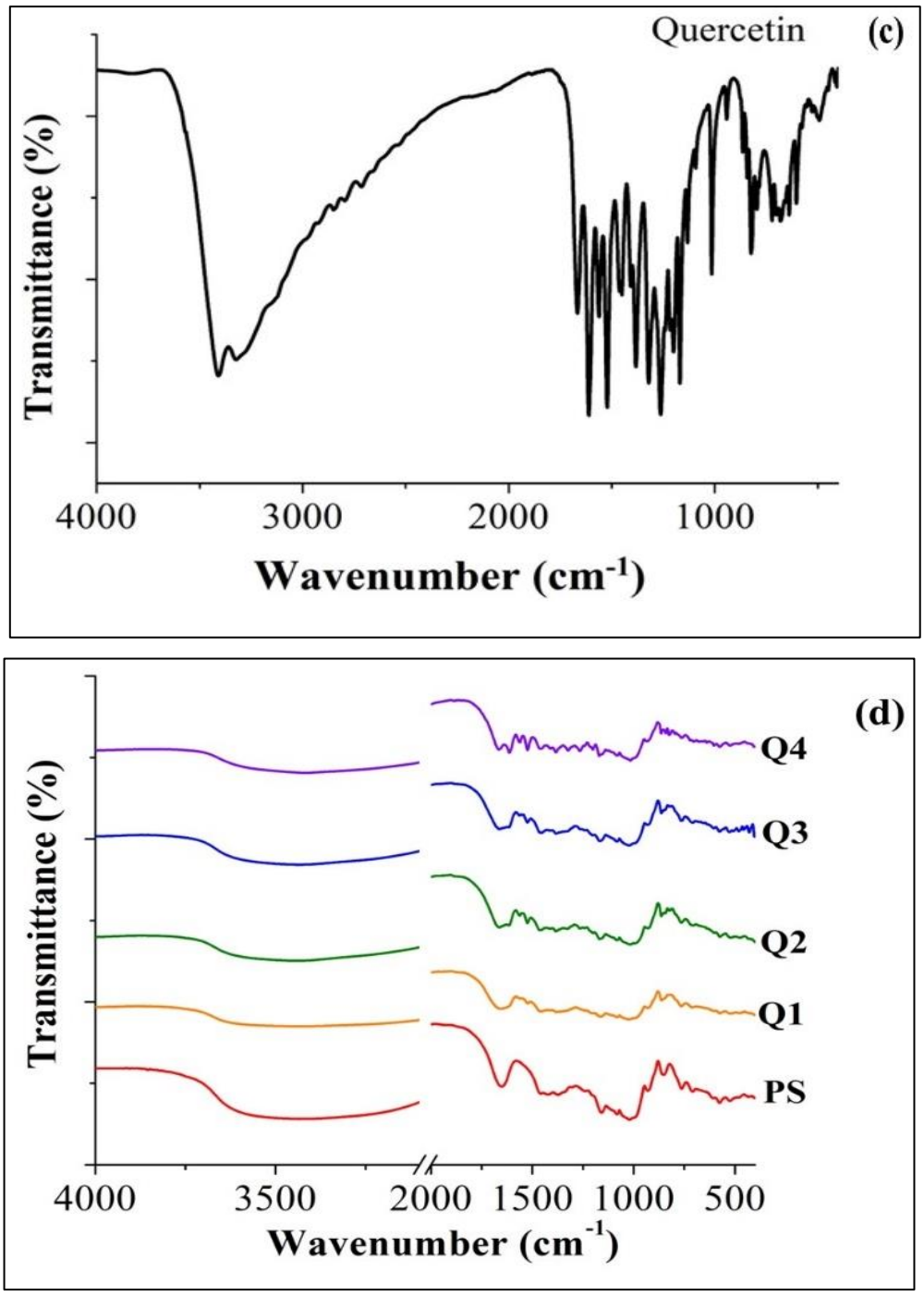

Fig. 4.4 (c) FTIR spectra of quercetin; **(d)** FTIR spectra of *Euryale ferox* kernel starch-quercetin complex

The FTIR spectra of quercetin [Fig. 4.4 (c)], and starch-quercetin complexes [Fig. 4.4 (d)] were recorded and presented. The absorption band observed at 2930 cm^{-1} found in starch, ferulic acid or quercetin molecules is due to the vibration of anti-symmetrical stretching of methyl (CH_2) [9, 20]. The broad peaks between 3000 cm^{-1} and 3600 cm^{-1} (O-H stretching) of control starch were shifted to 3441 cm^{-1} when ferulic acid was added and

3403 cm^{-1} when quercetin was added. Generally, the O–H stretching is used as a criterion to determine the stability of hydrogen bonding [35]. The phenol moiety of polyphenols might be responsible for the emergence of the new peak around 3400 cm^{-1} in the complexes [9, 20, 33]. The peak at around 3400 cm^{-1} in the complexes were broadened due to decrease number of hydroxyl groups [26]. It is because the hydrogen bond generated by the interaction of starch and polyphenols was stronger than the intermolecular hydrogen bond present in starch chains [14, 20, 37].

The band at 1648 cm^{-1}, which is linked to the absorbed water present in the amorphous region of starch was attenuated because more polar groups were exposed outside the hydrophobic cavity when ferulic acid penetrated the hydrophobic starch chamber [22]. A similar pattern was reported in potato starch-ferulic acid complex [26]. In *Euryale ferox* kernel starch-ferulic acid complex, many new peaks were emerged at 1823, 1662, 1621, 1519, 1514 indicating the presence of aromatic ring of ferulic acid caused by C-C skeletal vibrations. The CH_2 (methyl) bending vibration was signified by the band at 1465 cm^{-1}, while the vibration due to C-O-O stretching was represented by the band at 1433 cm^{-1}. Other new peaks appeared at 1377, 1326, 1289, 1272, 1204, 1113 cm^{-1}, were associated with benzene ring bond stretching [26]. Following quercetin complexation, there were several new peaks emerged at 1666, 1649 1613, 1563, 1526, 1459, 1393, and 1264 cm^{-1}, associated with benzene ring bond stretching [18, 28]. New absorption band at 1605 cm^{-1} in the EFKS-quercetin complexes, denotes the presence of C=O of the quercetin moiety [41].

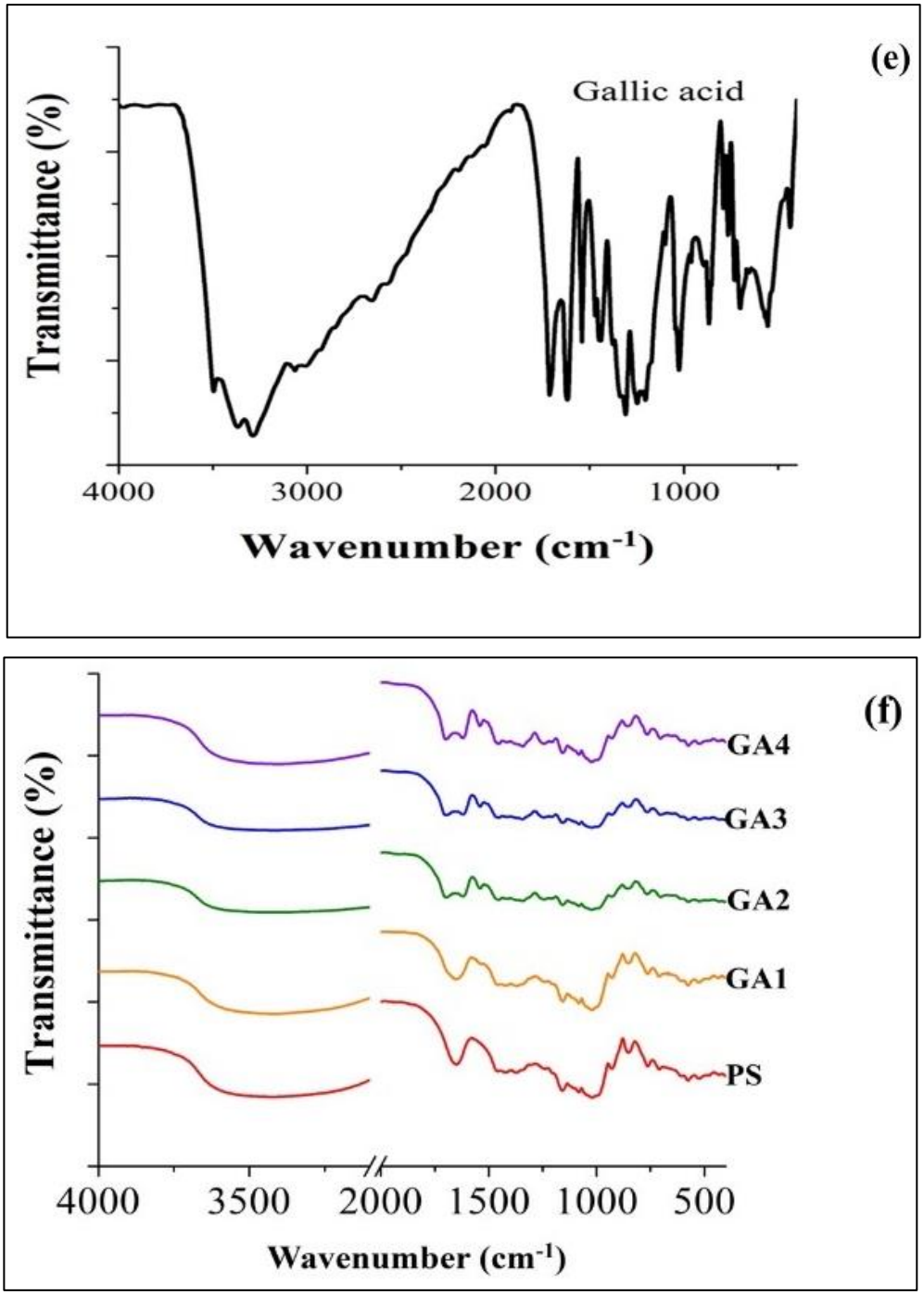

Fig. 4.4 (e) FTIR spectra of gallic acid; **(f)** FTIR spectra of *Euryale ferox* kernel starch-gallic acid complex

The FTIR spectra of GA [Fig. 4.4 (e)] showed the presence of C-O stretching vibrations at 1710 cm^{-1}, as well as new clear signals at 3292 cm^{-1} and 3501 cm^{-1} that were attributed to C-H stretching vibrations on unsaturated carbon and phenolic hydroxyl stretching vibrations. The FTIR spectra of EFKS-GA [Fig. 4.4 (f)] showed the emergence of new bands at 1696 cm-1 in contrast to EFKS. These bands were attributed to carbonyl C-O

vibrations of the phenyl ring of gallic acid. Some other new peaks were emerged at 3418 cm^{-1} (O−H stretching vibration), 1657 cm^{-1}, 1602 cm^{-1} (C = O stretching), 1505 cm^{-1} (C = C, aromatic), and 1362 cm^{-1} migrated from gallic acid

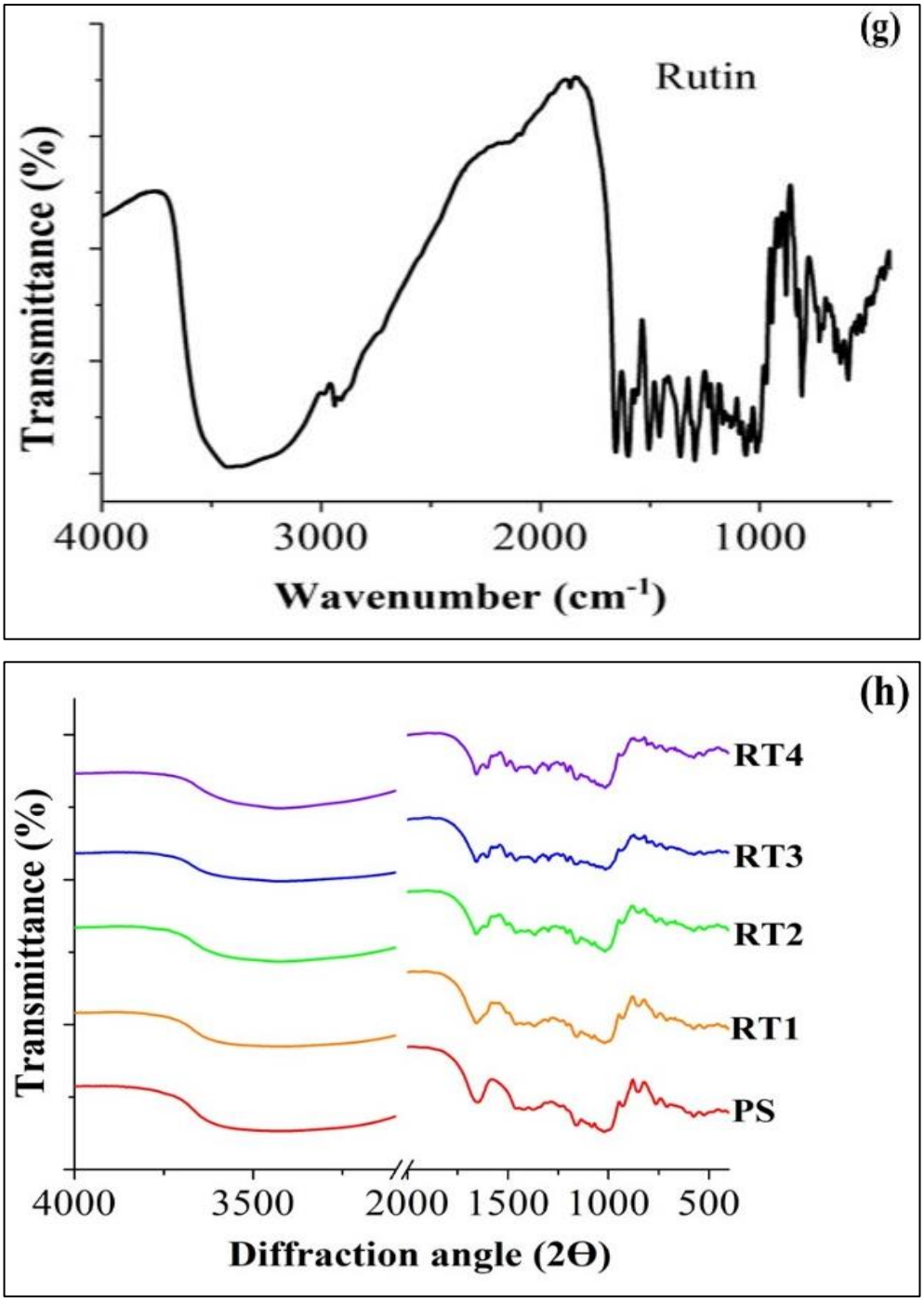

Fig. 4.4 (g) FTIR spectra of rutin; **(h)** FTIR spectra of *Euryale ferox* kernel starch-rutin complex

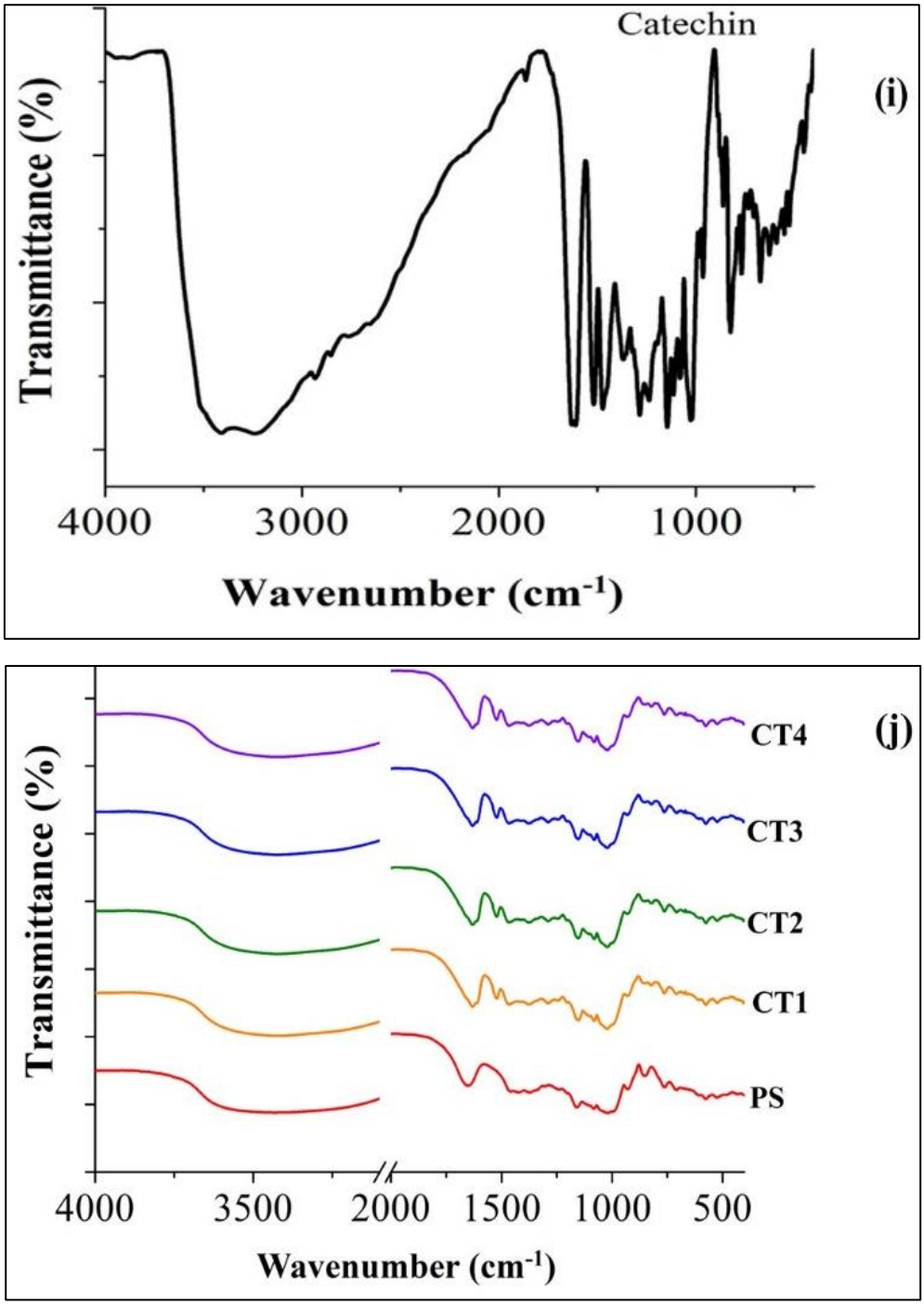

Fig. 4.4 (i) FTIR spectra of catechin; **(j)** FTIR spectra of *Euryale ferox* kernel starch-catechin complex

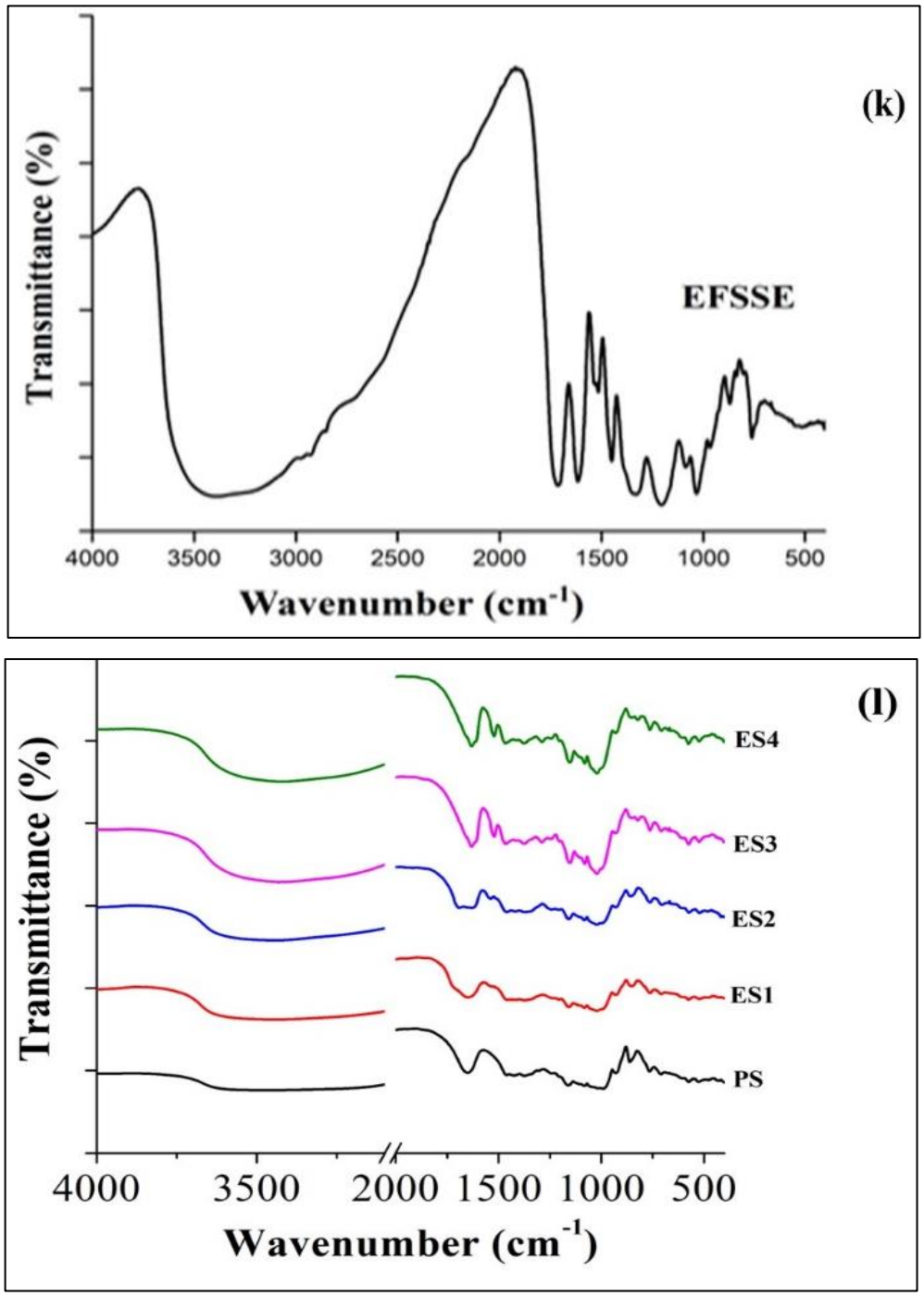

Fig. 4.4 (k) FTIR spectra of *Euryale ferox* seed shell extract; **(l)** *Euryale ferox* kernel starch-*Euryale ferox* seed shell extract complex

The FTIR spectra of rutin [Fig. 4.4 (g)] has exhibited vibration peak at 3441 cm^{-1} due to O-H stretching and the characteristics peak of rutin at 1655 due to the stretching vibrations of C=O, other peaks at 1598, 1502 cm^{-1} (C=C, aromatic); 1359 and 1295 cm^{-1} (C-O, phenolic group), 1200 cm^{-1} and 1063 cm^{-1} (C-O-C). In the EFKS-rutin complexes [Fig. 4.4

(h)], the O-H stretch shifted from 3405 cm^{-1} to 3450 cm^{-1}. The formation of hydrogen bonds between the molecules of EFKS and rutin may be attributed to the positional shifting of bands. The characteristics peak of rutin at 1665 cm^{-1} can be seen in the spectra of EFKS-rutin complexes, and it confirms the insertion of rutin into the complexes.

The FT-IR spectra of catechin [Fig. 4.4 (i)] displayed characteristics band at 3413 cm^{-1} due to O-H stretch, the C-H stretching at 2937 cm^{-1} and aromatic C=C stretching at 1608, 1520, and 1472. While the band at 1371 cm^{-1} was due to O-H bending and the presence of band at 1238 and 1283 cm^{-1} was due to C-C and C-O stretching respectively.

Catechins exhibited its peaks at 3412 cm^{-1}, 1636 cm^{-1}, 1284 cm^{-1}, 1143 cm^{-1}, and 1080 cm^{-1}which is attributed due to the existence of aromatic ring portion, O-H distortion of aromatic alcohol, C-O stretching of aromatic alcohol and aliphatic subsidiary alcohol, and C-O stretch respectively. The bands at 1080 cm^{-1} in the starch and catechin hydrate represents C-O-H bending. This C–O–H bending is frequently related to hydrogen bond formation. In case of EFKS-catechin complexes [Fig. 4.4 (j)], a minor shift of this wavenumber to a lower frequency (1014 cm^{-1}), indicating the presence of interactions between catechin and EFKS. Furthermore, the peak of catechin at 864 cm^{-1} due to benzene ring was observed in the complexes in a lesser intensity, which again confirms the interaction. Additionally, the complexes displayed several new peaks at 1526 and 1380 cm^{-1} due to C-C stretching of catechin. The abundance of phenolic hydroxyl groups in the catechin moiety also caused the O-H band at around 3400 cm^{-1}, to become wider.

The FT-IR spectra of EFSSE [Fig. 4.4 (k)] demonstrated its polyphenolic nature. In, EFKS-EFSSE complex [Fig. 4.4 (l)], the shifting and disappearance of absorption peaks indicating possible interaction. Based on our findings and some of the previous similar investigations, EFKS has interacted with polyphenols through non-covalent bonds, and an intermolecular H-H bond is thought to be responsible [41]. The variations in FT-IR spectra revealed that the principal interactions between different polyphenols and starch differ according to the molecular structure, and type of phenolic compounds [14, 19].

4.3.1.3 ^{1}H-NMR spectroscopy

^{1}H-NMR spectroscopy was performed to explore the interaction between starch and polyphenols at the molecular level. The ^{1}H NMR spectra of ferulic acid [Fig. 4.5 (a)], starch [Fig. 4.5 (b)], and starch-ferulic complexes [Fig. 4.5 (c)] were recorded. The signal

peaks of DMSO and water molecules were detected at 2.49 and 3.33 ppm, respectively. The proton signals of starch were detected at 5.49 (3-OH), 5.40 (2-OH), 5.11 (1-H), and 4.57 ppm (6-OH). The protons detected in the range of 4.5 to 5.6 ppm are associated with anomeric and hydroxyl protons of starch monomers. The proton signals at 3.64, 3.36 and 3.33 ppm were related to 2-H to 6-H of anhydro glucose units [38]. The ^{1}H NMR spectra of ferulic acid exhibited signals in the range of 6.54-8.06 associated with the aromatic ring and phenolic hydroxyl groups [6, 30]. Unlike the control starch, the ^{1}H NMR spectra of starch-ferulic acid showed multiple additional peaks between 6.00-9.00 ppm corresponding to its methine protons [36]. There were multiple peaks between 2.8 and 3.4 ppm but no sharp peaks between 6 and 8 ppm (phenyl protons) up to 5% level of incorporation indicating low inclusion of polyphenols. The signal intensities of aromatic ring and phenolic hydroxyl protons emerged between 6-9 ppm in starch-ferulic acid complexes escalated with the increased level of ferulic acid addition. In addition, the signal intensities of free hydroxyl protons at 5.4 and 5.5 ppm in starch-ferulic acid complexes decreased after complexation because the carboxyl of ferulic acid reacted with free hydroxyl (OH-2, OH-3, or OH-6) to create complex via hydrogen bonds [36].

These proton signals suggested that ferulic acid had entered the starch cavity, possibly with some of its unsaturated and aromatic moieties. It was reported that the OH groups of starch and the carboxyl group of polyphenols, form intermolecular H-bonds both, which occur on the exterior surface of the starch [15]. Similar results were reported, suggested a noncovalent interaction between starch and ferulic acid through hydrophobic interaction, hydrogen bonding, and electrostatic interaction [20]. It was reported that CH-π bond was responsible for the interaction between aromatic residues of polyphenols and pyranose rings of starch. The strength of CH-π bond is related to the strength of the aromatic ring of polyphenols [6, 19].

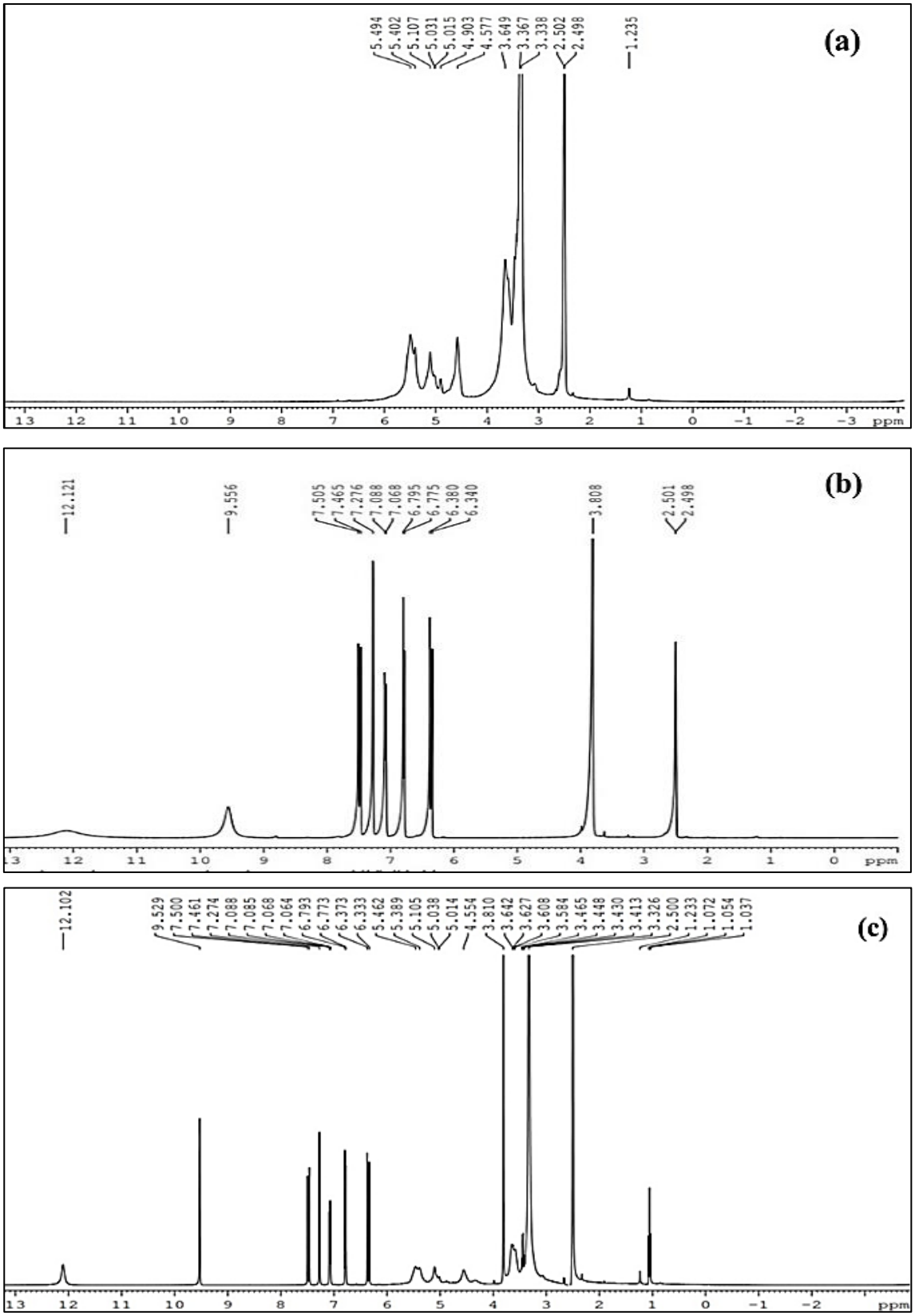

Fig. 4.5 (a) ^{1}H NMR spectra of pregelatinized- *Euryale ferox* kernel starch; **(b)** ^{1}H NMR spectra of ferulic acid; **(c)** ^{1}H NMR spectra of *Euryale ferox* kernel starch-ferulic acid (2.5%) complex

The ^{1}H NMR spectra of quercetin [Fig. 4.5 (d)], and starch-quercetin complexes [Fig. 4.5 (e)] are presented. The proton signals of quercetin at 6.19 ppm and 6.41 ppm in the ^{1}H NMR spectra were associated with the H-6 and H-8 in the A-ring of quercetin, whereas the peaks at 6.89 ppm, 7.55 ppm, and 7.68 ppm were associated to H-5′, H-6′, and H-2′ of the B-ring. ^{1}H NMR spectra of the starch-quercetin complexes exhibited a significant proton shift at the aromatic region. The intensities of characteristic aromatic proton signal peaks shifted to the lower field in comparison to pure quercetin. However, as the amount of quercetin addition increased, the strength of these new signals eventually became higher. It has also been shown in earlier research that polysaccharide-quercetin complexes exhibit the distinctive protons of the quercetin moiety [38].

Although, B-ring protons were reported to be less active as compared to A-ring protons, it has been shown that EFKS-quercetin complexation occurs through both the A and B rings of the compound. Incorporating labile protons from phenolic hydroxyl into hydrogen bonds was successful. As a result, the oxygen in hydroxyl group became more negatively charged, which increased the density electrons in the benzene ring and the C=C bond and led the peak to move to the up field. In the case of the complexes, the outcome showed that the intramolecular hydrogen bonding disappeared and the aromatic protons of quercetin were clearly moved up field. Quercetin exhibited an up-field shift, showing that the hydroxyl group in B rings had priority in forming hydrogen bonds. The proton signals also moved to the up field as a result of the phenolic proton's reduced electron density brought on by hydrogen bond in the starch hydroxyl groups and the following π-π interaction impact of the decentralized electrons on the benzene ring. Nevertheless, the complexation most likely took place in carboxyl groups of phenolic acids and hydroxyl groups of glucose residues. According to a recent study, quercetin complexes can form through both the A and B rings of the compound, however the B-ring protons were lesser active than the A-ring protons [23].

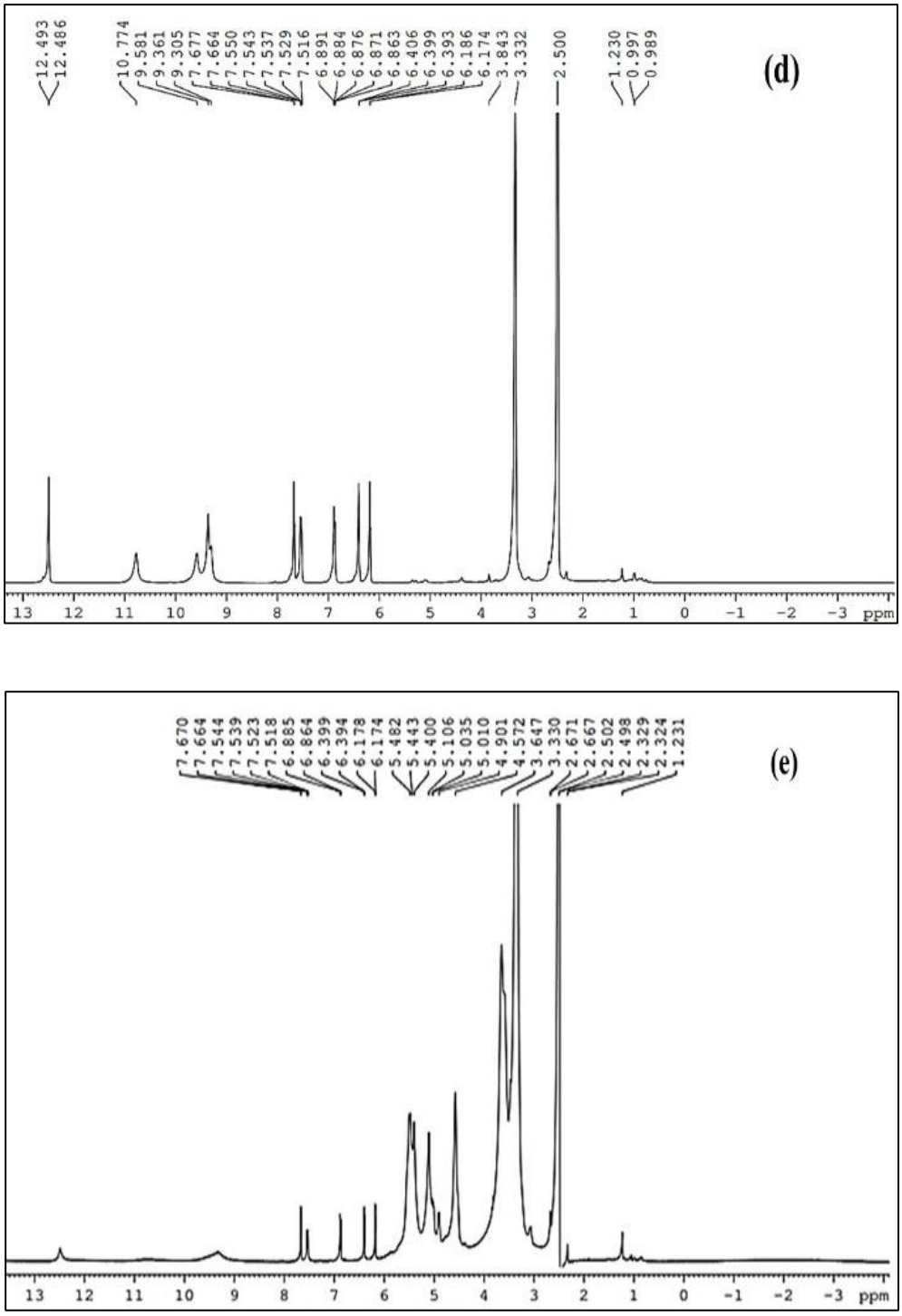

Fig. 4.5 (d) ^{1}H NMR spectra of quercetin; **(e)** ^{1}H NMR spectra of *Euryale ferox* kernel starch-quercetin (2.5%) complex

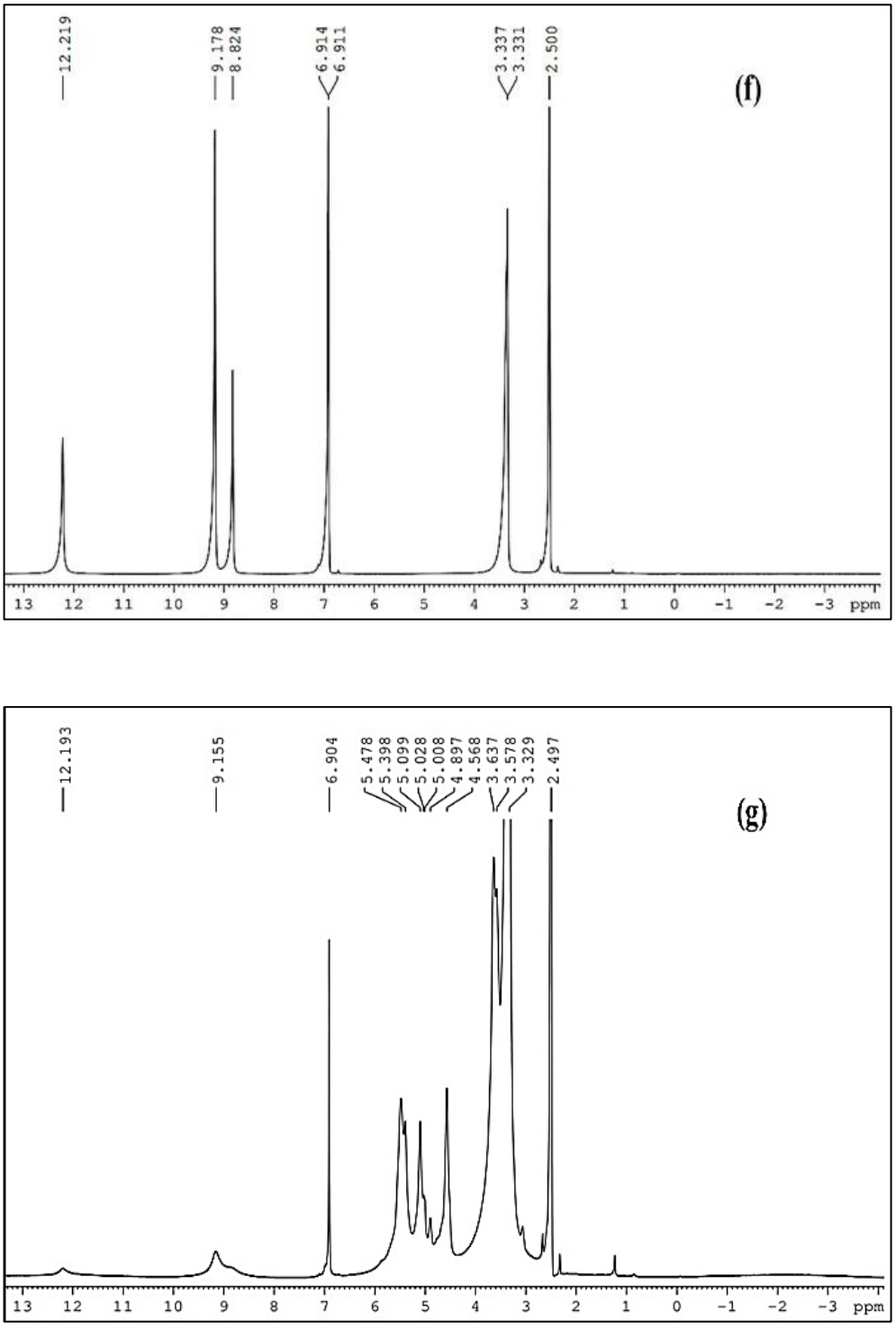

Fig. 4.5 (f) ^{1}H NMR spectra of gallic acid; **(g)** ^{1}H NMR spectra of *Euryale ferox* kernel starch-gallic acid (2.5%) complex

The ^{1}H NMR spectra of gallic acid [Fig. 4.5 (f)], and starch-gallic acid complexes [Fig. 4.5 (g)] are presented. The spectra of EFKS-gallic acid complexes included all the peaks of EFKS and emergence of a new peak around 7.1 ppm that comes from gallic acid phenyl

protons, confirming the successful implantation of gallic acid onto starch via its hydroxyl groups on C-6. It was further confirmed that there was no unreacted gallic acid in the complex as the peaks at 7.4–8.0 ppm, which are indications of gallic acid, did not show up in the spectra.

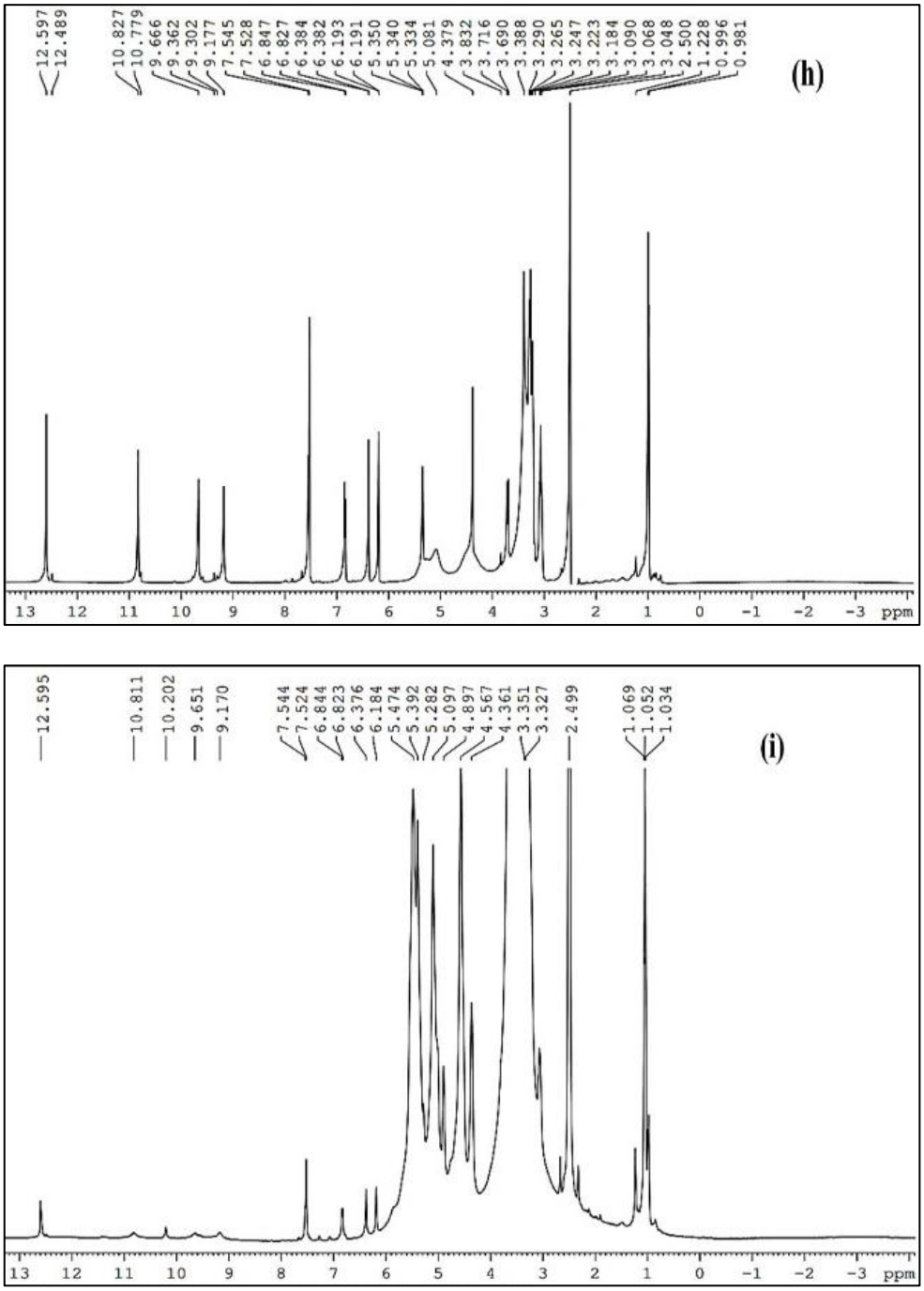

Fig. 4.5 (h) ^{1}H NMR spectra of rutin; **(i)** ^{1}H NMR spectra of *Euryale ferox* kernel starch-rutin (2.5%) complex

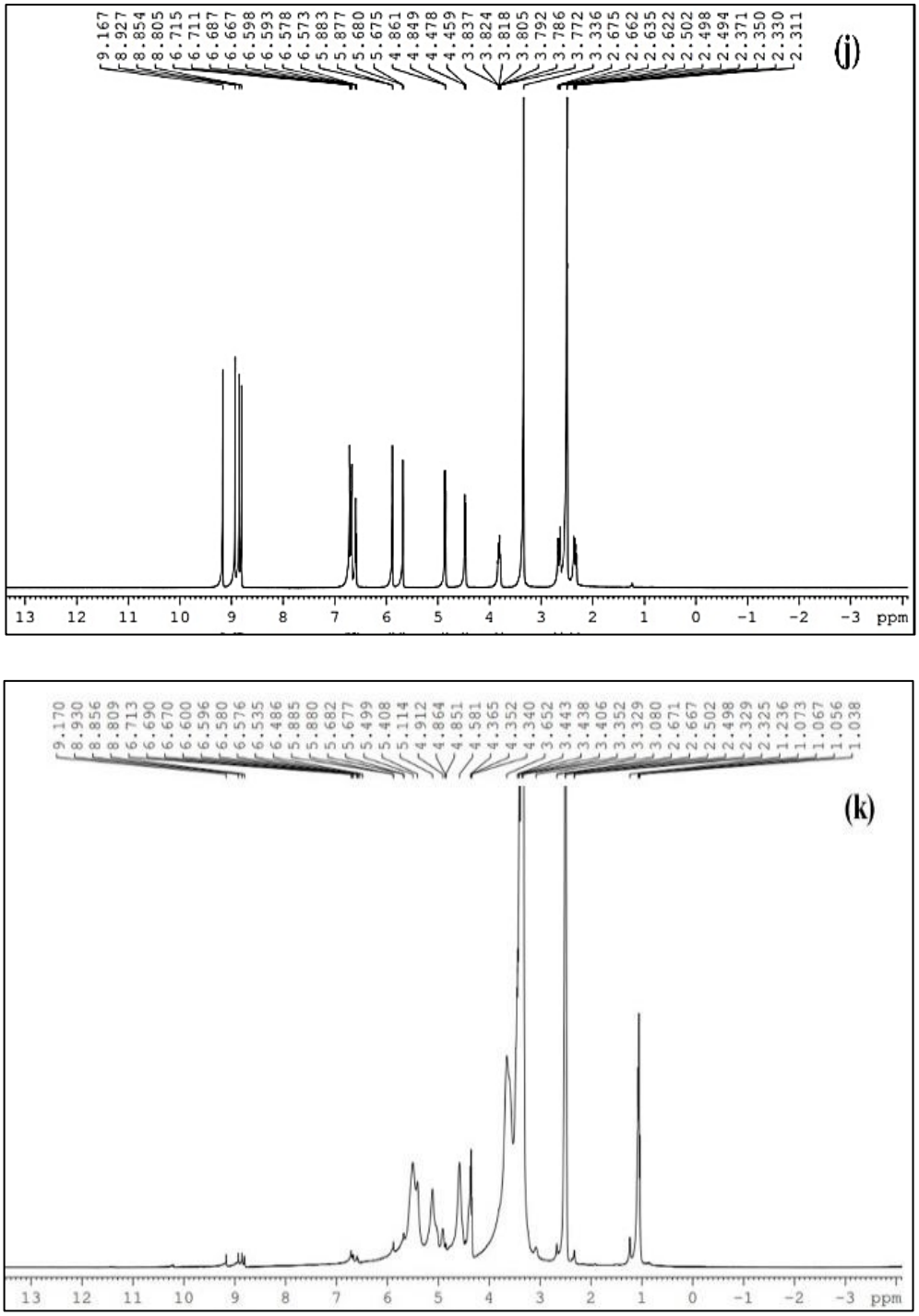

Fig. 4.5 (j) ^{1}H NMR spectra of catechin; **(k)** ^{1}H NMR spectra of *Euryale ferox* kernel starch-catechin (2.5%) complex

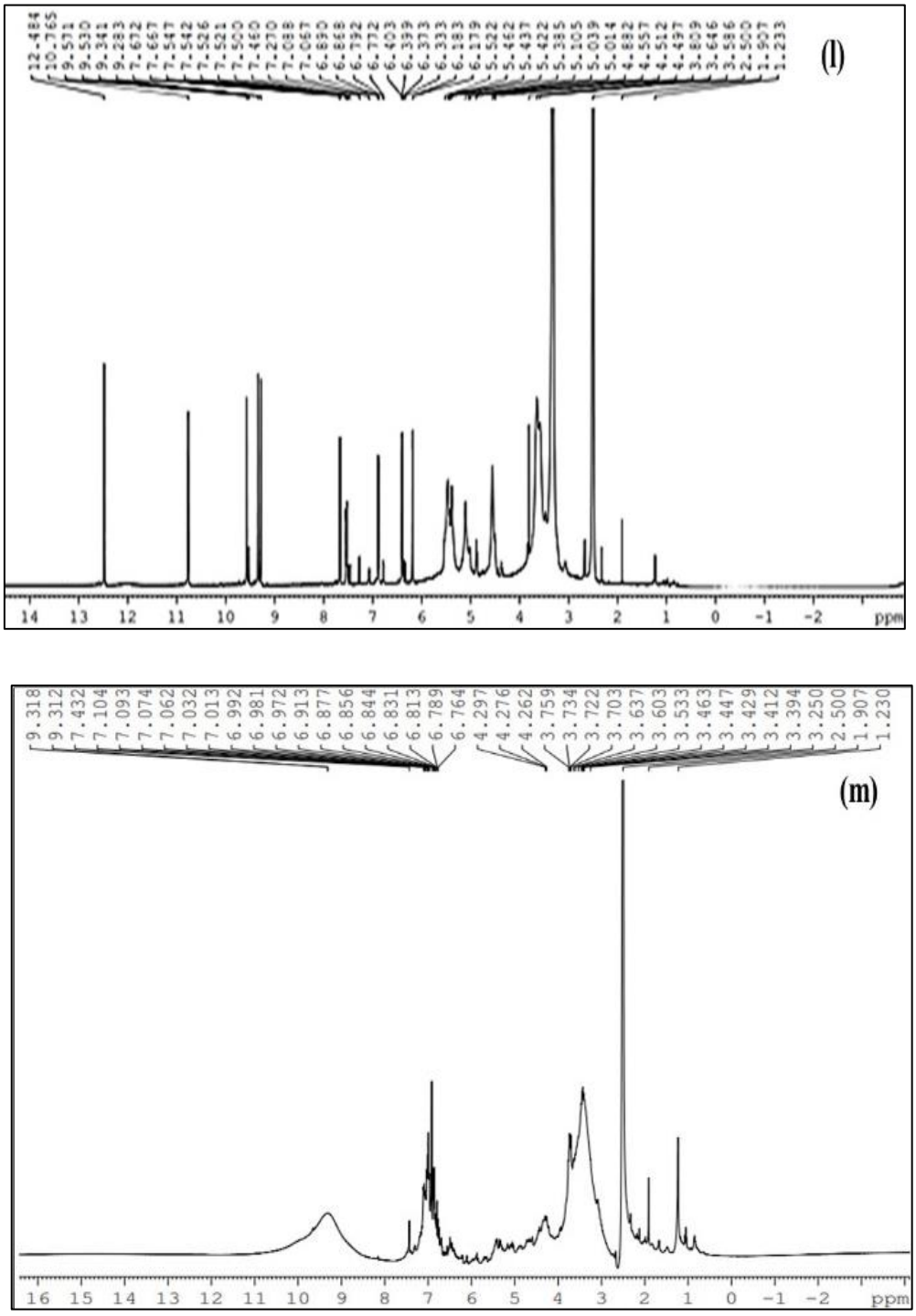

Fig. 4.5 (l) ^{1}H NMR spectra of EFSSE (*Euryale ferox* seed shell extract); **(m)** ^{1}H NMR spectra of *Euryale ferox* kernel starch-*Euryale ferox* seed shell extract (2.5%) complex

The ^{1}H NMR spectra of rutin [Fig. 4.5 (h)], and starch-rutin complexes [Fig. 4.5 (i)] were displayed. The aromatic protons of rutin can be seen from its ^{1}H NMR spectrum. The carboxylic group of the rutin was linked to the hydroxyl group of the starch, to obtain EFKS-rutin complex [Fig. 4.5 (i)]. The hydroxyl of *Euryale ferox* kernel starch and the

phenol fraction of rutin reacted to form EFKS-rutin complex. The A ring protons at H6 and H8 may easily be attributed to peaks at 6.234 and 6.39 ppm, whereas the peaks at 6.91, 7.67, and 7.70 ppm, respectively are associated with the H5', H60, and H20 of B ring protons demonstrating that the B ring of rutin interacts with the duo sugar moieties by hydrogen bond [27].

The ^{1}H NMR spectra of catechin [Fig. 4.5 (j)], and starch-rutin complexes [Fig. 4.5 (k)] were displayed. The protons designated for 5–OH at 8.94, 7–OH at 9.18, 3'–OH at 8.87, and 4'–OH at 8.82 in catechin were shifted to 9.06, 9.33, 8.95 and 8.89, while 3–OH at 3.84 disappeared, confirming that the complexation occurred at 3–OH of C-ring. Several proton signals were observed for catechin at = 6.87 ppm (H-2), 6.84 ppm (H-5), 6.78 ppm (H-6), 6.02 ppm (H-6), 5.87 ppm (H-8), 4.64 ppm (H-2), 4.09 ppm (H-3), 2.77 and 2.45 ppm (H-4) [16]. New peaks in the EFKS-catechin complex between 6.32 and 8.22 for C-2, C-5, C-6, C-7 and C-8 were observed compared to the unmodified starch. This confirms the complexation of catechin onto the starch backbone. In contrast to starch, starch-catechin complexes displayed new signals around 6.80 ppm, which were associated with the catechin B-rings H-2′, H-5′, and H- 6′. However, no catechin A-ring proton signals (around 6.0 ppm) were seen, indicating that the complexation took place via the H-6 and H-8 of the catechin A-ring. According to the results above, the catechin A-ring's H-6 and H-8 undergone complexation. Activated A-ring was mainly employed to attach catechin to starch [23].

The ^{1}H NMR spectra of EFSSE [Fig. 4.5 (l)], and EFKS-EFSSE complex [Fig. 4.5 (m)] were presented. The findings of the present study demonstrated that the complexation location of starch-polyphenols complex was affected by the nature of polyphenol. The fact that the compounds were only partially dissolved in the solvents may be the cause of the low substitution degree [2]. In comparison to free flavonoids, the protons signal of the complexes is shifted to lower frequencies. This is most likely induced by the complex formation, which increases the planarity of the flavonoid molecules and causes a conjugation effect to rise. The resonances of the 3-OH ad 7-OH groups of hydroxyls are absent in the complexes of quercetin, rutin, and catechin complexes. These findings indicate that the OH protons were lost during complexation [28].

4.3.1.4 Differential Scanning Calorimetry (DSC) analysis

Differential scanning calorimetry (DSC) has been regarded as a useful method for investigating the interactions between starch and polyphenols. The thermal characteristics of the polyphenols and their starch-complexes were examined and are depicted in Fig. 4.6. The introduction of new peaks, shifting of peaks, loss of endothermic peaks is used to infer the nature of interaction.

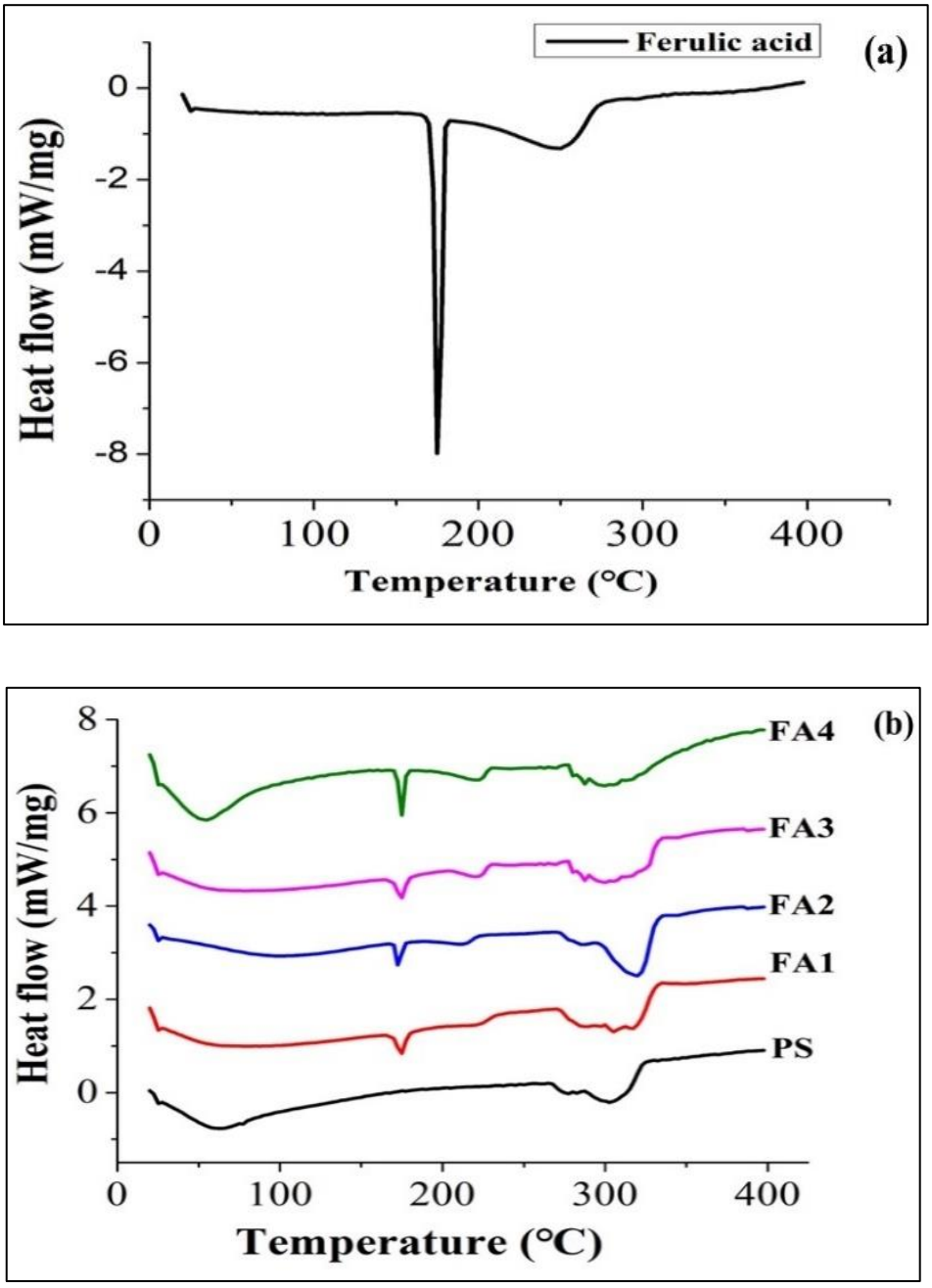

Fig. 4.6 (a) DSC thermogram of ferulic acid; **(b)** DSC thermogram of *Euryale ferox* kernel starch-ferulic acid complex

The DSC curve of ferulic acid [Fig 4.6 (a)] showed a sharp endothermic peak at 176°C and broad peaks at around 317°C, associated with dehydration and melting point, respectively. On the other hand, the DSC thermogram of EFKS [Fig. 4.6 (b)] exhibited two endothermic peaks, a broad endothermic peak between 60 and 100°C, which is associated with the loss of water, and the other peak at around 310°C, which is associated with the breakdown of inter-and intra-molecular hydrogen bonds and the decomposition of starch backbone chains. The DSC profiles of starch-ferulic acid complexes showed a series of temperature shifts that were comparable to those observed for starch and ferulic acid. In EFKS-ferulic acid complexes, the endothermic peak related to water loss was shifted to lower temperature (52.47°C), indicating ferulic acid attachment decreases the water-holding capacity of starch.

In the EFKS-ferulic acid complexes, the endothermic peaks emerged at around 172 °C was close to the melting point of ferulic. Following complexation, the hydroxyl portion of starch chain were substituted by the hydroxyl groups of ferulic acid. However, the limited hydroxyl groups and limited size of ferulic acid is responsible for the interaction. Therefore, a part of the ferulic acid may adhere on the surface of starch granules and undergo thermal breakdown at around 172°C.

The results of the current study, thus, demonstrated that the ferulic acid-starch complexes underwent thermal breakdown at the pyrolysis temperature of ferulic acid. Complexation could increase the intermolecular hydrogen bonds between molecules, which is associated with the rise in thermal stability of starch due to the increased crystallinity thereby hindering the heat and mass transfer. The shifting and widening of the characteristic peak are an indication that the structure has altered and further confirmed that ferulic acid was successfully attached to starch [18].

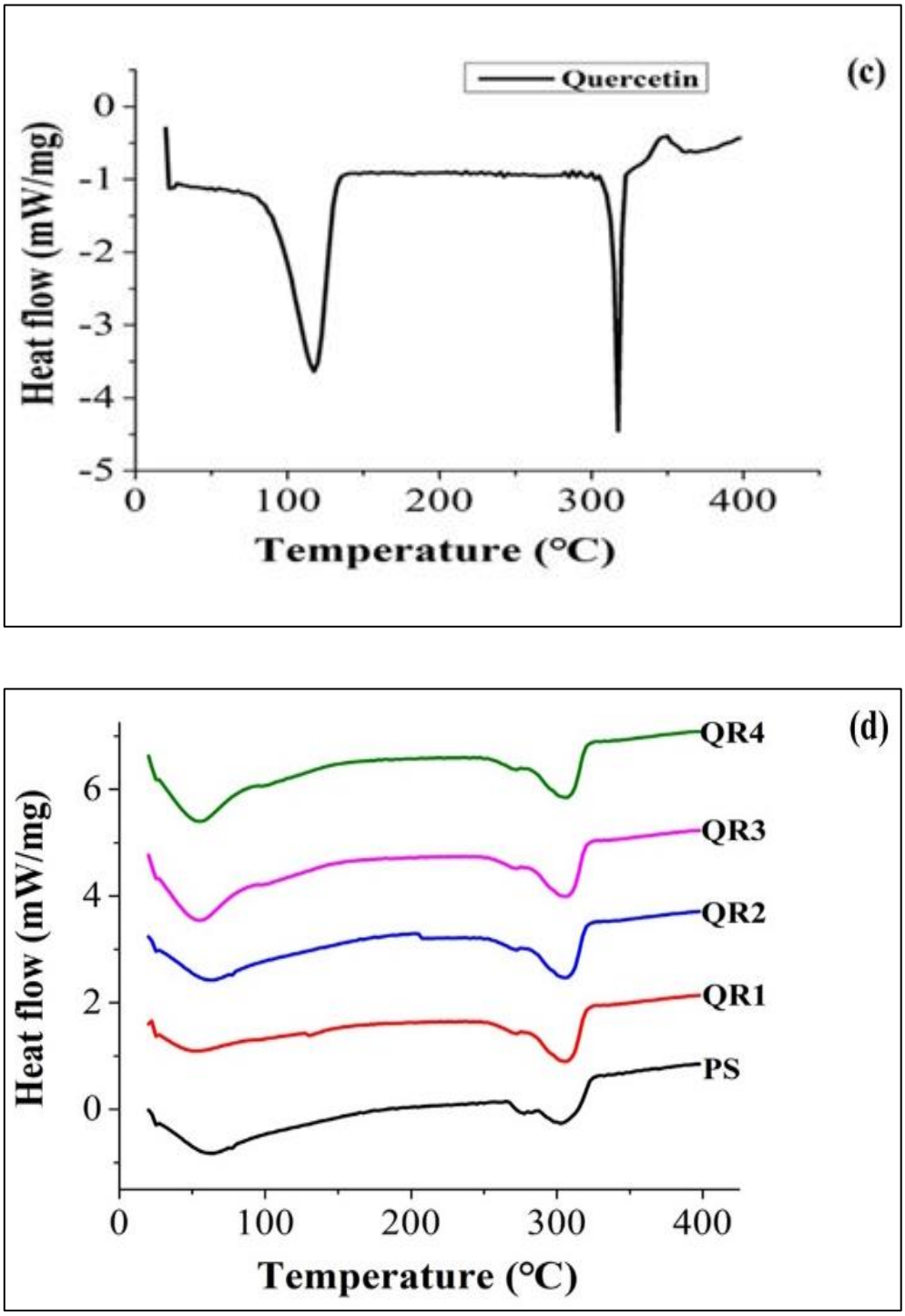

Fig. 4.6 (c) DSC thermogram of quercetin; **(d)** DSC thermogram of *Euryale ferox* kernel starch-quercetin complex

The DSC thermogram of quercetin [Fig. 4.6 (c)] showed a broad endothermic peak at 117°C and sharp endothermic peaks at 317°C corresponding to dehydration and melting of quercetin, respectively. EFKS-quercetin complexes [Fig. 4.6 (d)] did not bring much

significant changes other than the wide endothermic peak, which is associated with the release of bound water from. *Euryale ferox* kernel starch-quercetin complexes did not show any thermal transitions corresponding to the melting point of quercetin, and also the other characteristics peaks of quercetin at 117℃ and 317℃ was disappeared. It is important to disclose that the amount of quercetin level had no identifiable effect on the transition temperature. This phenomenon suggested a strong interaction between the two substances and the creation of a new phase. In this case, quercetin was fully dispersed inside the starch matrix and thus reduces its crystallinity.

The compact semi-crystalline structure of the complexes is probably responsible for the change in thermal stability and similar results have been reported [6]. Amorphous structures require less energy due to their randomly organized molecules, hence easily soluble [40]. Moreover, the single helix structure of starch is more prone to disruption than other structures, leading to a lower gelatinization temperature. The hydroxyl and carboxyl groups on the starch chain interacted with polyphenols via hydrogen bonds or hydrophobic interactions. Our finding suggests that varying degrees of interaction and/or amorphization in complexes is related to differences in polyphenols solubility [18].

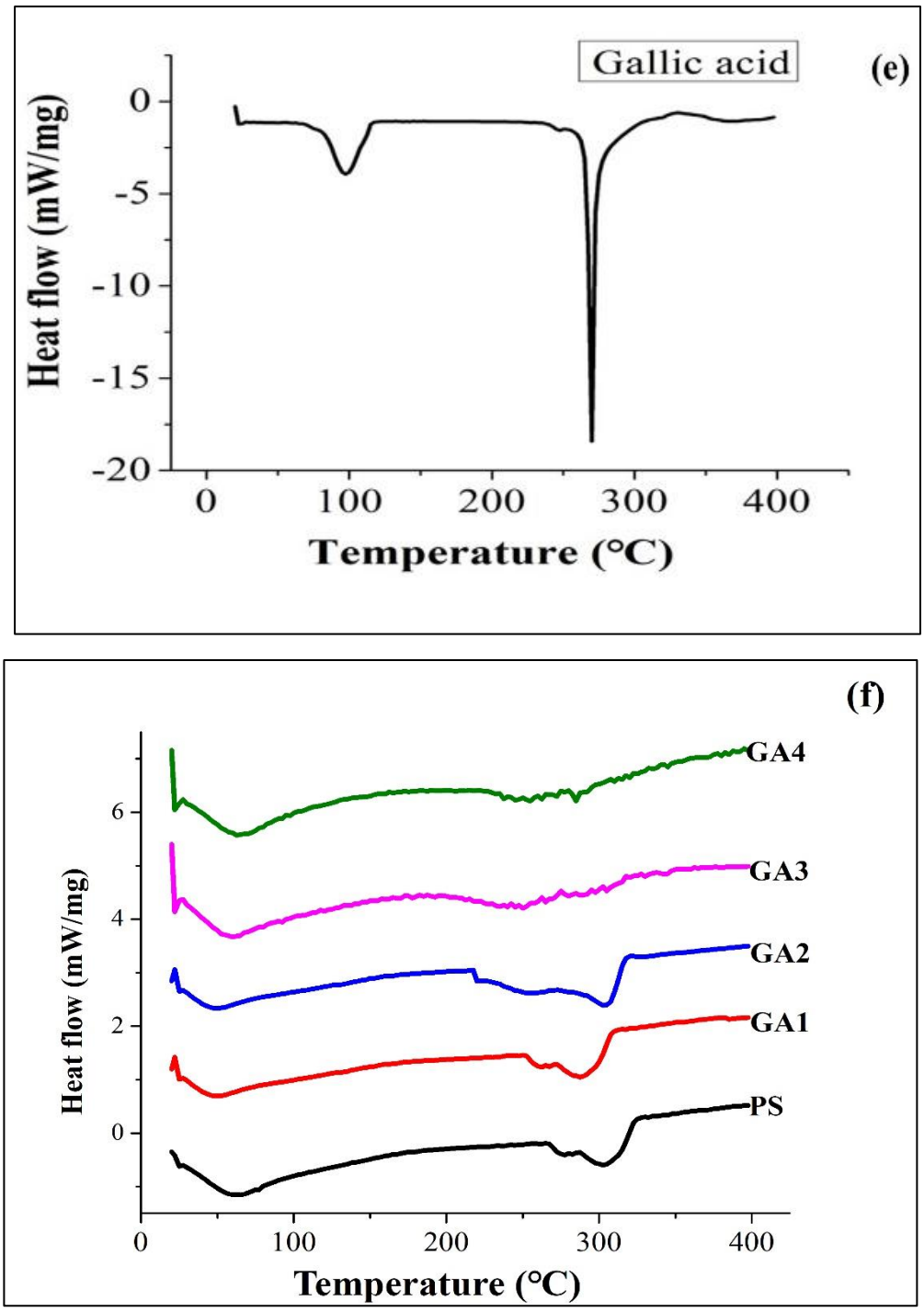

Fig. 4.6 (e) DSC thermogram of gallic acid; **(f)** DSC thermogram of *Euryale ferox* kernel starch-gallic acid complex

The DSC thermogram of gallic acid [Fig. 4.6 (e)] had a sharp-edged endothermic peak at 269 °C, associated with the melting point of gallic acid. The DSC thermogram of EFKS-gallic acid complex [Fig. 4.6 (f), revealed that the endothermic peak of the complexes

including the GA1, GA2, GA3 and GA4 shifted to 79.6, 77.7, 76.53, and 73.6 ℃, respectively, showing that addition of GA moieties to the starch backbone reduced water holding capacity. The intermolecular hydrogen bonding between molecules decreased following complexation, which likely contributed to the decrease in the thermal stability of EFKS-gallic acid complexes. The decrease in the crystallinity of EFKS-gallic acid, which was observed in the XRD pattern, complements the result. As a result, EFKS-gallic acid might have superior solubility than the control starch.

Gallic acid (GA), starch, and the EFKS-gallic acid complex all began to thermally degrade at 254, 264, and 254℃, respectively. This data therefore demonstrated that the EFKS-gallic acid complexes underwent thermal breakdown at the pyrolysis temperature of gallic acid at 254℃, prompting to infer that the combusting component was the gallic acid of the complexes. The hydroxyl and carboxyl groups on the starch chain created hydrogen bond with gallic acid. However, the limited hydroxyl groups and tiny size of gallic acid were responsible for the weak interaction between starch and gallic acids [3]. This behavior may reduce water mobility and hinder gelatinization process [15]. In the starch-gallic acid complexes, there was no discernible peak of gallic acid. An increase in melting stability suggests that EFKS-gallic acid may require more heat energy for gelatinization. Similar results regarding the endotherms of starch gelatinization properties in the presence of phenolic chemicals have been reported [6].

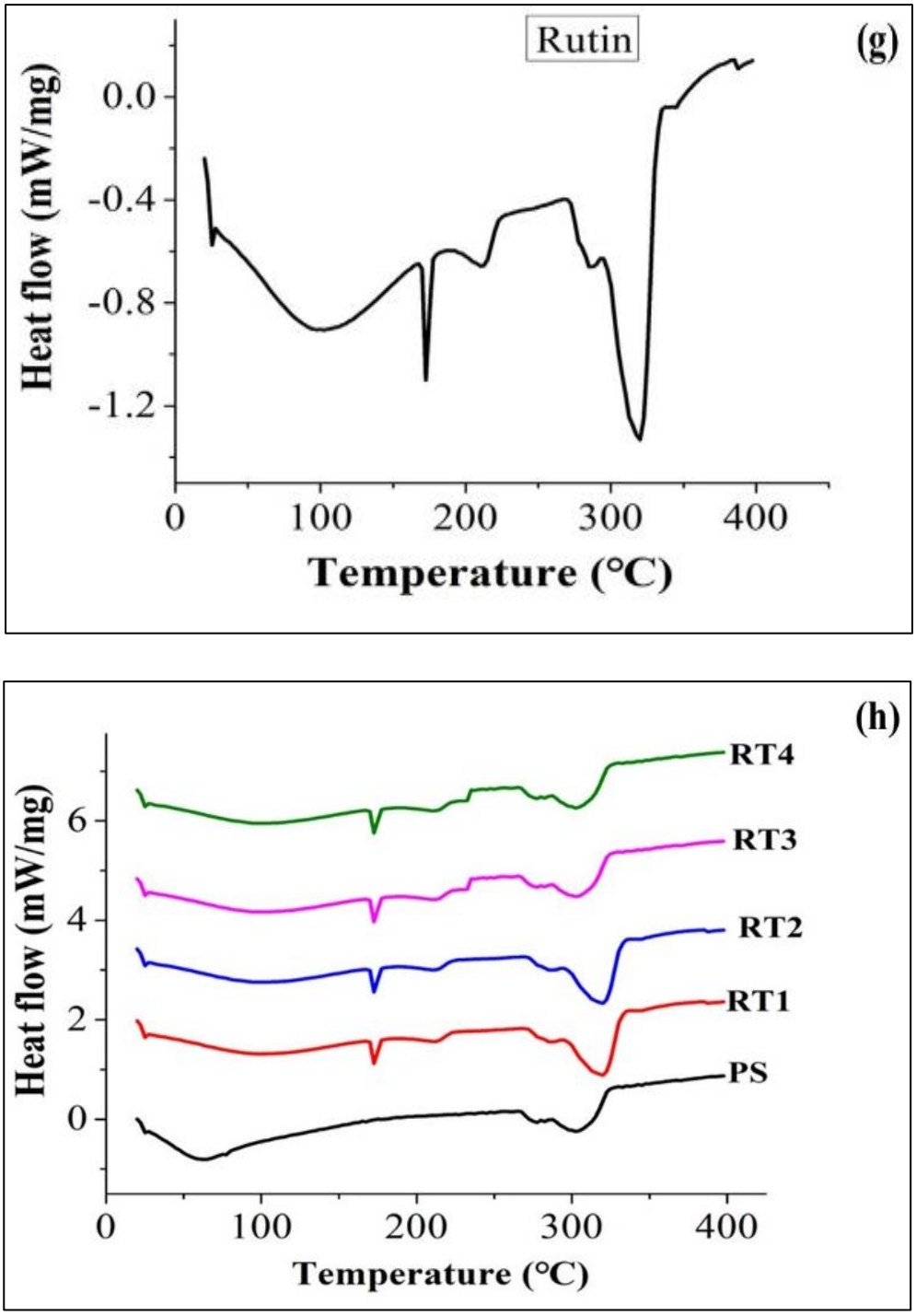

Fig. 4.6 (g) DSC thermogram of DSC thermogram of rutin; **(h)** DSC thermogram of *Euryale ferox* kernel starch-rutin complex

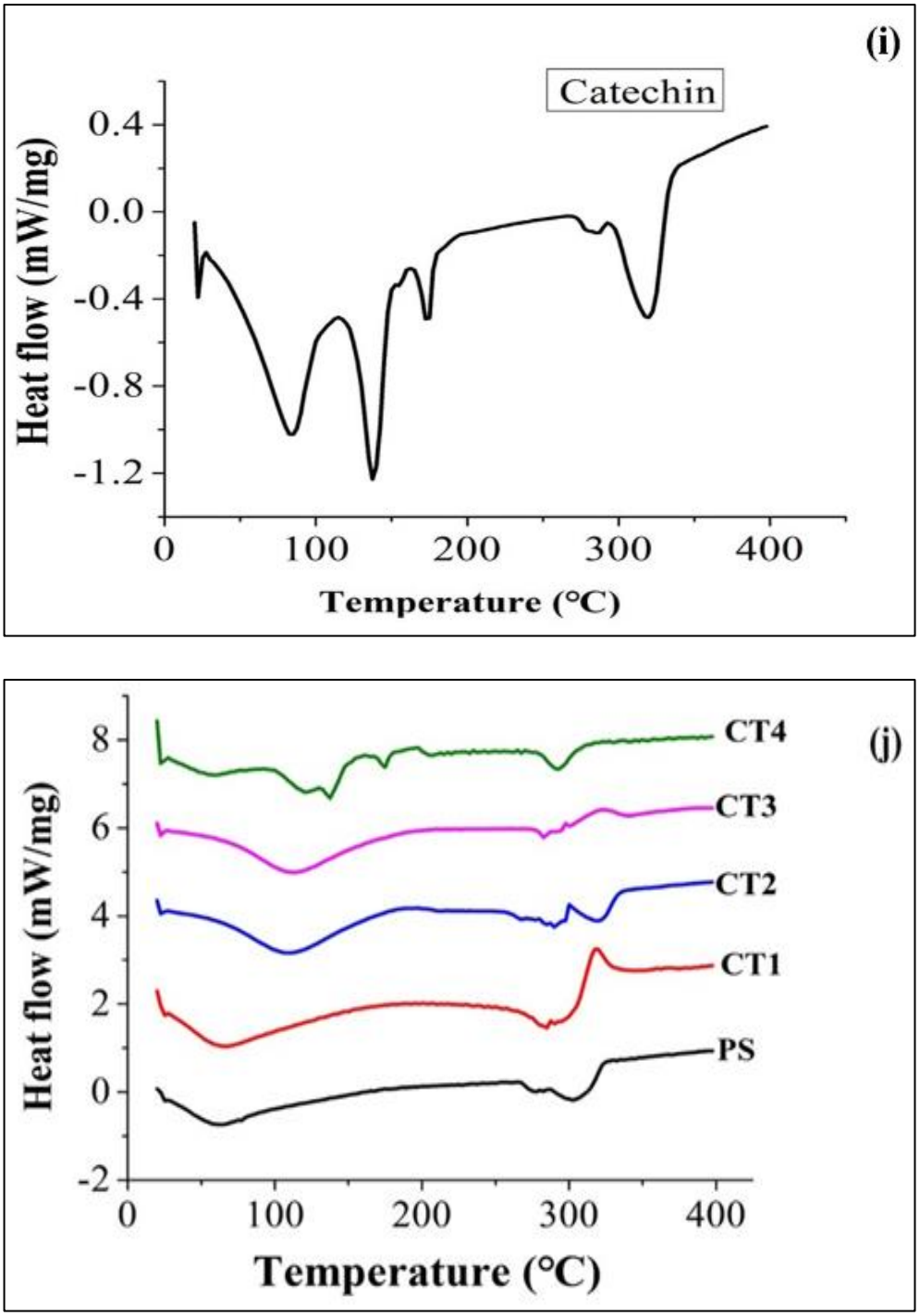

Fig. 4.6 (i) DSC thermogram of catechin; **(j)** DSC thermogram of *Euryale ferox* kernel starch-catechin complex

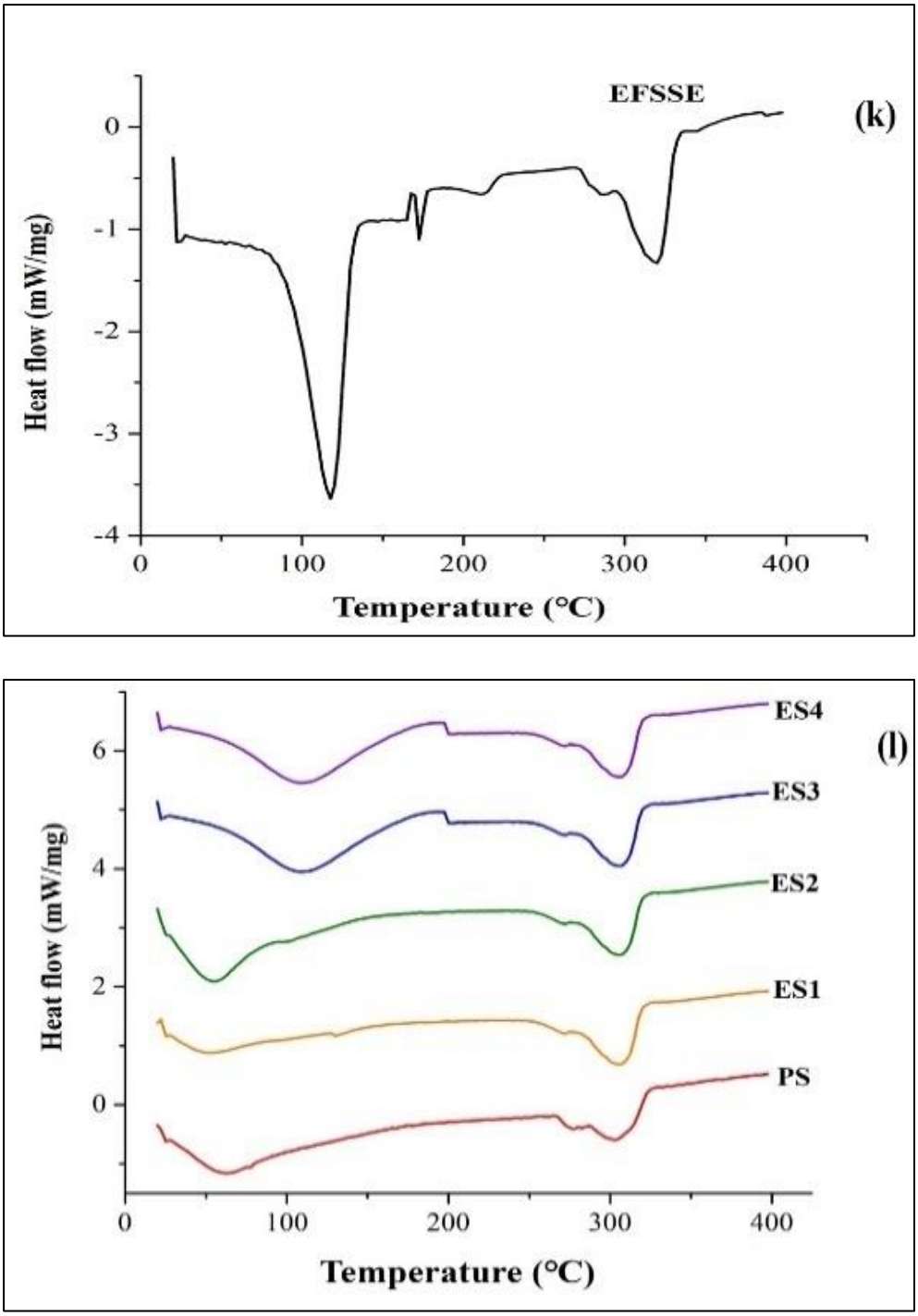

Fig. 4.6 (k) DSC thermogram of *Euryale ferox* seed shell extract; **(l)** DSC thermogram of *Euryale ferox* kernel starch-catechin complex

Pure rutin exhibited a clear and distinct endothermic peak at 190.25℃, which is the melting temperature of rutin [Fig. 4.6 (g)]. The first endothermic peak of rutin was detected in the temperature range between 77.46 to 97.79 °C, due to the release of bound water from the rutin molecules. The other three peaks at 210.28, and 319℃ corresponding to its decomposition. Whereas, EFKS-rutin complexes [Fig. 4.6 (h) underwent thermal

breakdown at 190.25℃, prompting to infer that the combusting component was the rutin of the complexes. After complexation, the existence of rutin embedded within the starch matrix is indicated by the broader glass transition peaks of the complexes, which demonstrated greater heterogeneity due to the melting of a variety of molecular weights. From the DSC curve, it was observed that the interaction with starch caused the two endothermic peaks to disappear and shift towards higher temperatures. This finding implies that rutin is molecularly dispersed in the starch matrix, which further confirms the trapping of rutin inside the amorphous portion of starch [28]. A higher degradation temperature is an indication of improved structural perfection and increased stability. This demonstrated that complexation offered thermal protection of rutin molecules. Similar findings have also been previously reported [28].

The DSC curves for catechin [Fig. 4.6 (i)] revealed the endothermic transitions peak at 82 and 137℃, which correspond to the dehydration of the hydrated catechin, 173 and 280℃, associated to the melting point of catechin crystalline solids, and 319℃ is associated with the decomposition of catechin molecule. The DSC curves for EFKS-catechin complexes [Fig. 4.6 (j)] did not exhibit any thermal transitions corresponding to pure catechin, rather a displaced endothermic peak that matched the glass transition temperature of starch. These findings suggest that catechin is distributed inside the polymeric matrix of starch in an amorphous form. However, there were shifting in the positions of these transition peaks and a few newly produced signals at 10% level of incorporation were detected; these shifts in peak positions imply that interactions between starch and polyphenols resulted to the production of a different structural organization of the starch and polyphenols.

Catechin could decrease the melting stability, lowering the amount of thermal energy needed for hydration. Further, catechin might limit the availability of water for hydration and movement, which would result in lower melting temperature than the control. The results were consistent with those found in the literature, showing that catechin complexation significantly reduced the thermostability of processed starch samples by weakening the chain interactions and external chain length in crystalline/amorphous lamella. This reduced the ability of amylopectin to hydrate and accelerated gelatinization for the primary endotherm of starch from various botanical sources [28]. According to DSC curves, the thermal degradation temperatures for the EFKS-catechin complexes was in the range of 315-318℃, demonstrating that the thermal stability of starch was reduced.

The DSC thermogram of EFSSE is presented Fig. 4.6 (k) and Fig. 4.6 (l) respectively. In case of EFKS-*Euryale ferox* seed shell extract complex, there were no significant changes in the complexes. The DSC thermogram of the complexes suggested that the EFSSE were thoroughly distributed inside the polymeric matrix of starch in an amorphous form.

4.3.1.5 Scanning electron microscopy (SEM) analysis

The impacts of various polyphenols on the morphological structure of *Euryale ferox* kernel starch granules were examined using SEM. The surface of the native EFKS was smooth, and free of holes or openings, although the dimensions of the starch granules were not uniform. However, when *Euryale ferox* kernel starch was gelatinized, it disintegrated into tiny clumps with uneven surfaces (Fig. 4.7). Swelling and rupturing of starch granules during the process of gelatinization and short-term retrogradation disrupted the morphology [3].

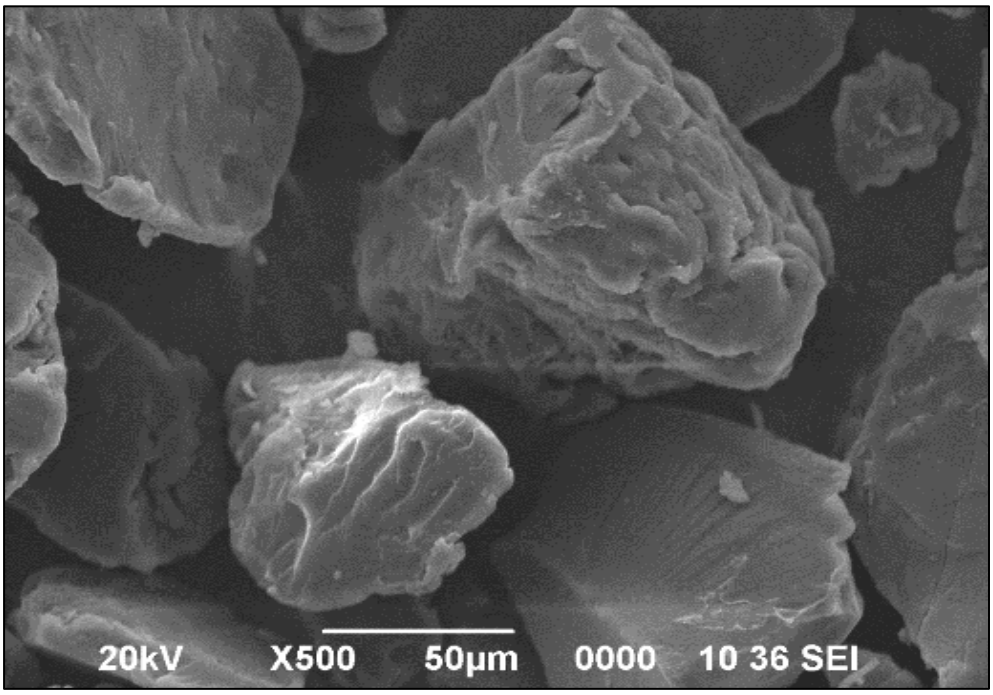

Fig. 4.7 SEM micrographs of pregelatinized *Euryale ferox* kernel starch

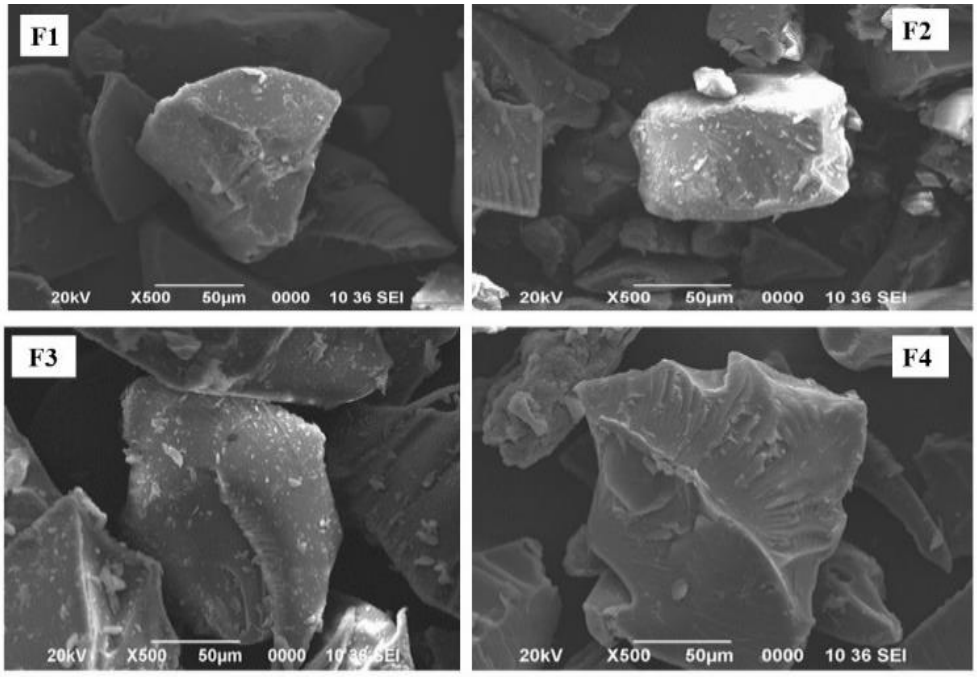

Fig. 4.8 SEM micrographs of *Euryale ferox* kernel starch-ferulic acid complex, F1, F2, F3 and F4 indicated *Euryale ferox* kernel starch complexed with 2.5, 5, 7.5 and 10 g ferulic acid per 100 g starch respectively

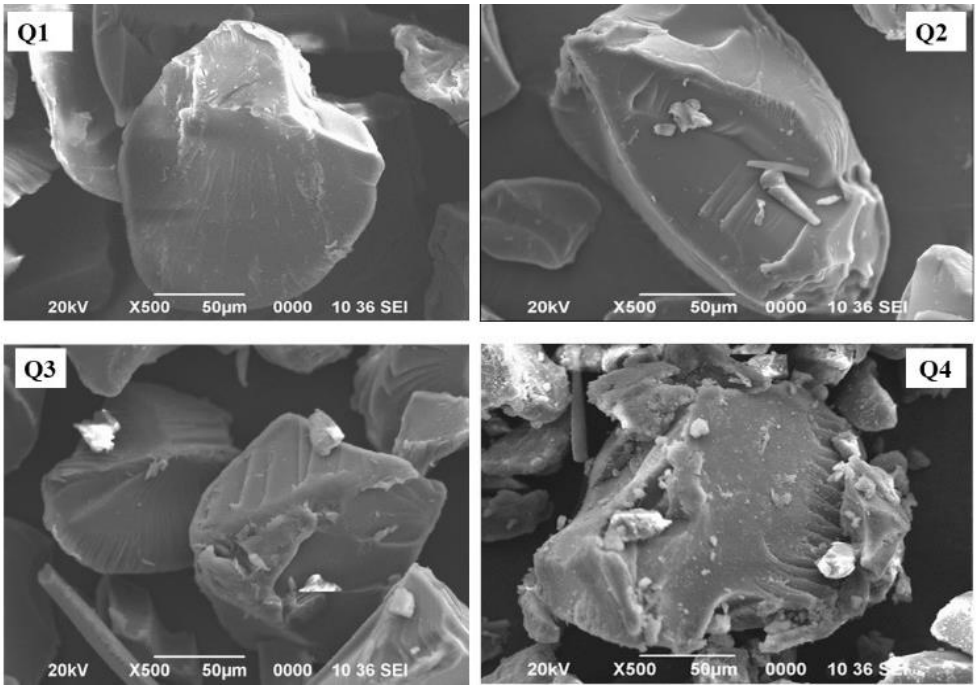

Fig. 4.9 SEM micrographs of *Euryale ferox* kernel starch-Quercetin complex; Q1, Q2, Q3 and Q4 indicated *Euryale ferox* kernel starch complexed with 2.5, 5, 7.5 and 10 g Quercetin per 100 g starch respectively

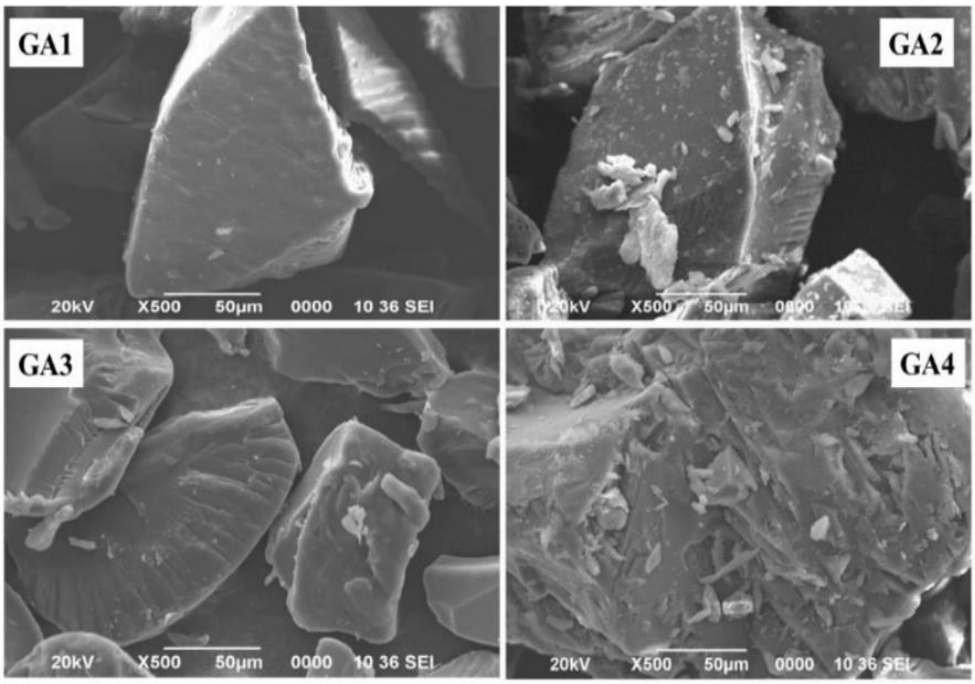

Fig. 4.10 SEM micrographs of *Euryale ferox* kernel starch-gallic acid complexes; GA1, GA2, GA3 and GA4 indicated *Euryale ferox* kernel starch complexed with 2.5, 5, 7.5 and 10 g gallic acid per 100g starch respectively

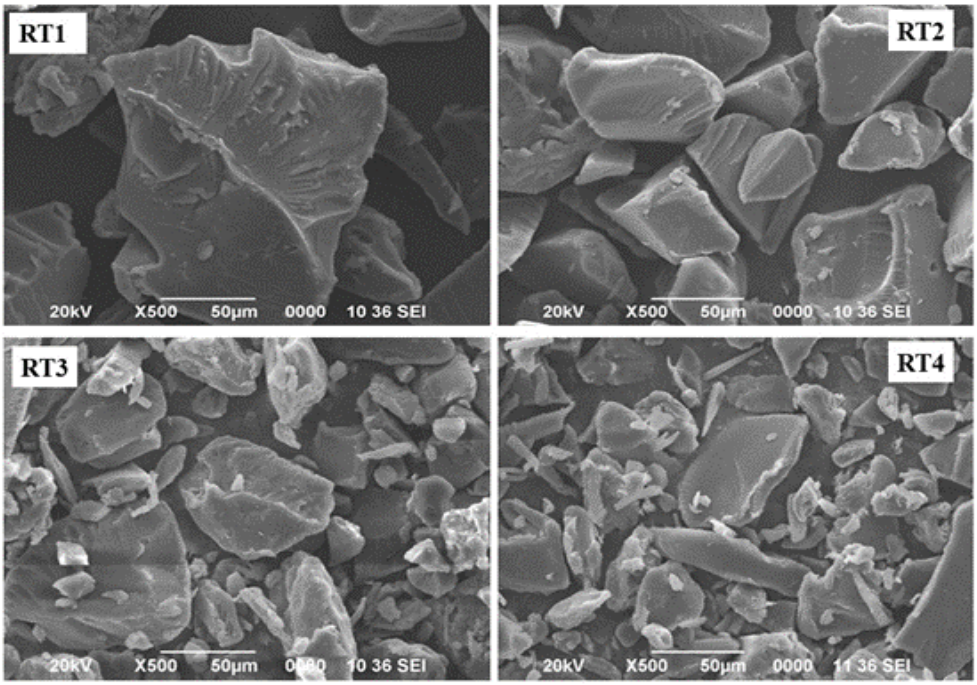

Fig. 4.11 SEM micrographs of *Euryale ferox* kernel starch-rutin complexes; RT1, RT2, RT3 and RT4 indicated *Euryale ferox* kernel starch complexed with 2.5, 5, 7.5 and 10 g rutin per 100 g starch respectively

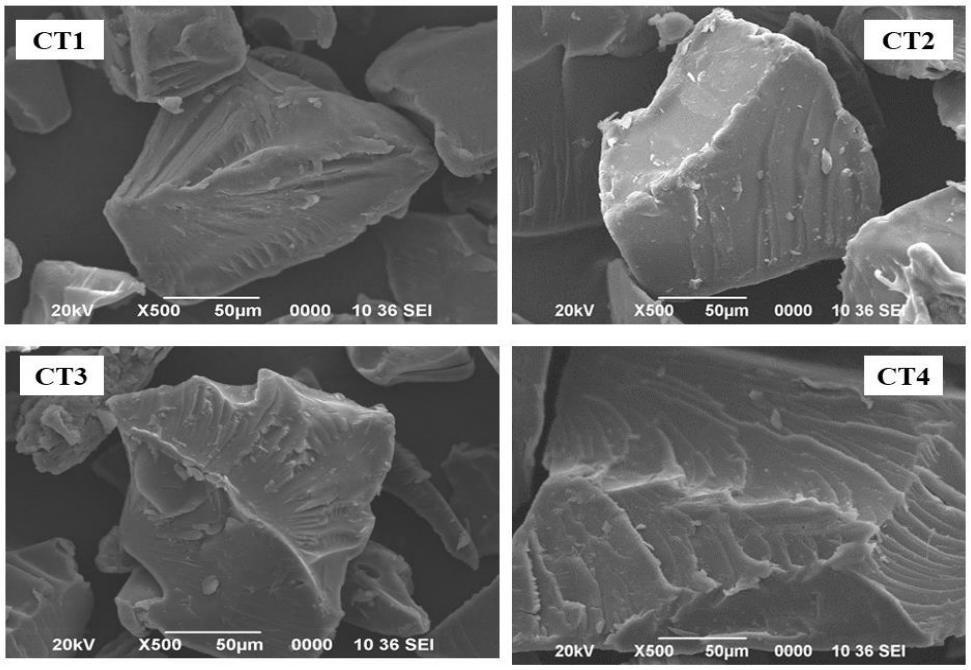

Fig. 4.12 SEM micrographs of *Euryale ferox* kernel starch-catechin complexes; CT1, CT2, CT3 and CT4 indicated *Euryale ferox* kernel starch complexed with 2.5, 5, 7.5 and 10 g catechin per 100 g starch respectively

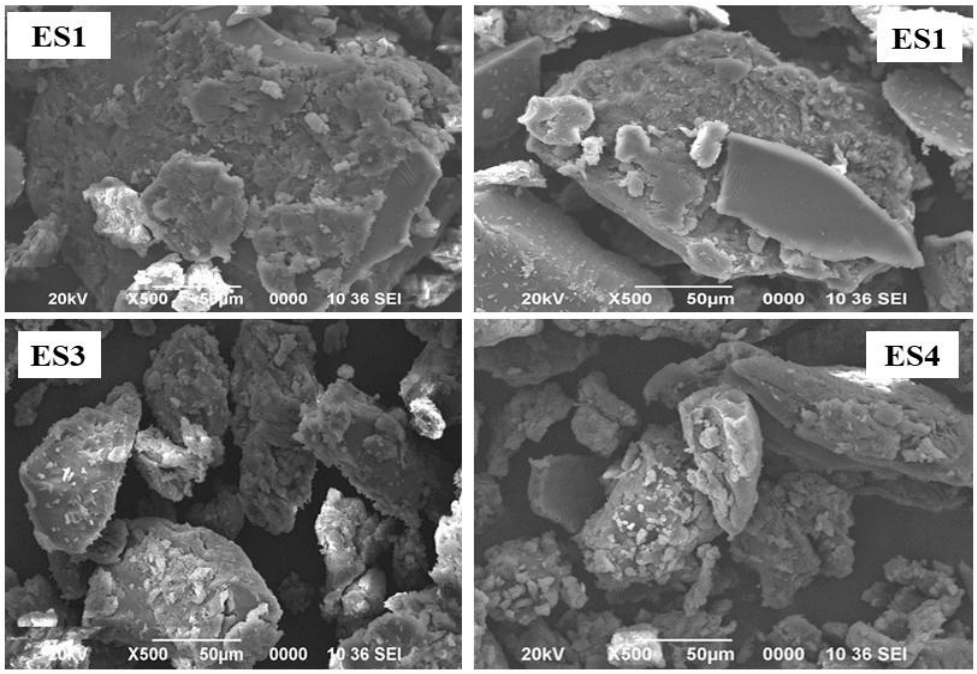

Fig. 4.13 SEM micrographs of *Euryale ferox* kernel starch-*Euryale ferox* seed shell extract complexes; ES1, ES2, ES3 and ES4 indicated *Euryale ferox* kernel starch complexed with 2.5, 5, 7.5 and 10 g *Euryale ferox* seed shell extract per 100 g starch respectively

Addition of polyphenols, entangles the chains of *Euryale ferox* kernel starch, guest compounds were visible on the surface, which suggest that polyphenols could change the structural configuration. Increased concentration of ferulic acid promoted the development of holes in the complexes, which can be seen in case of F4 (Fig. 4.8). Starch-polyphenols interactions generally occurred on the granule surface [1]. Zhao et al. (2019) [42] found that the surface morphology of green tea polyphenol added lotus seed starch complexes resulted tightly compressed structure.

In the SEM micrographs, it can be observed that the adherence of quercetin to *Euryale ferox* kernel starch granules transformed the morphology (Fig. 4.9). This phenomenon happens due to the hygroscopic nature of polyphenols embedded in the complexes, which helps to prevent water evaporation and retain the microstructure [14]. Additionally, the hydrothermal conditions employed during the complexation might be responsible for the structural alterations on the surfaces of starch granules [10].

The insertion of polyphenols enabled the starch granules to agglomerate to a greater extent, which suggested that the two substances greatly increased the cross-linking of the starch granules and generated a stable colloidal suspension after gelatinization [41]. However, it was observed that the starch granules became looser and rougher as the concentration of polyphenols reached 10%, the starch granules collapsed. This change in morphology revealed that polyphenols not only interfere with the cross-linking of starch chains but also disrupts the structural configuration during the complexation process [10]. The addition of polyphenols produced smooth surface granules unlike the porous pre-gelatinized starch. It may be because phenolic compounds work as a plasticizer inducing the amorphous and semi-crystalline area to developed into more organized and compact [10].

4.3.2 *In vitro* starch digestibility

4.3.2.1 Starch fractions

The percentages of RDS, SDS, and RS of the pregelatinized *Euryale ferox* kernel starch and the developed complexes are shown in Table 4.1. Pre-gelatinized EFKS (PS) exhibited 77.34%, 14.97%, and 7.69% of RDS, SDS, and RS, respectively. As anticipated, addition of polyphenols could significantly reduce RDS fraction while increasing the SDS and RS fraction in the complexes dose dependently. There was a wide difference in the RDS content among the complexes, the highest RDS content (61.25%) was found in ES4

(*Euryale ferox* kernel starch + 2.5% *Euryale ferox* seed shell extract) while the lowest RDS (20.97%) content was exhibited by *Euryale ferox* kernel starch + 10% ferulic acid. Since RDS causes instant blood sugar spikes and insulin levels, which is linked to the obesity, diabetes, and cardiovascular diseases [1]. On the other hand, SDS is responsible for steady release of glucose and higher satiety value, thus desirable. It suggested that the RDS fraction might have changed into the SDS and RS fractions. Regardless of the types of polyphenols, the SDS concentration increases with the increased level of polyphenol addition but varied significantly amongst complexes. The SDS proportion, which was 14.97% in the control starch however increased to 35.75% in GA4 (*Euryale ferox* kernel starch + 10% gallic acid), was significantly increased. At the end of the hydrolysis, the lowest resistant starch fraction was observed in ES1 (*Euryale ferox* kernel starch + 2.5% EFSSE) while the highest resistant starch content (54.68 %) was exhibited by Q4 (*Euryale ferox* kernel starch + 10% quercetin). The findings of our study indicated that the complexation of polyphenols onto *Euryale ferox* kernel starch produced resistant starch even in its gelatinized form.

Polyphenols complexation could enhance the long-range crystallinity of starch granules as observed in XRD patterns, which is accountable for greater resistance to enzymatic breakdown. The reduced granule swelling of the complexes increases the viscosity, producing a denser network, reduces the flowability, thus hindering the accessibility of hydrolytic enzymes, and thus increases the resistant starch fraction [13]. Polyphenols bind to starch by occupying its hydrophobic helical domain rendering a more compact structure which retard the rate of starch hydrolysis [32]. Polyphenols frequently interacted with α-amylase or α-amyloglucosidase via hydrogen bonds and Van Der Waals interaction at their catalytic sites, hence the responsiveness of these enzymes is inhibited [37]. Moreover, the release of attached polyphenols from the complex during the course of digestion inhibit the further digestion [7]. In short, the reduced digestibility was not only rendered by increase in crystallinity, but also the activity of polyphenols. One mechanism most certainly does not conflict with the other, rather act synergistically [11].

Table 4.1 Starch fractions of *Euryale ferox* kernel starch-polyphenol complex

Sample	**RDS (%)**	**SDS (%)**	**RS (%)**
PS	77.34 ± 2.07^{a}	14.97 ± 2.01^{a}	7.69 ± 1.00^{a}
F1	54.33 ± 0.80^{bcde}	24.59 ± 0.83^{def}	21.07 ± 1.50^{bc}
F2	45.33 ± 2.19^{efgh}	26.02 ± 2.18^{efg}	28.64 ± 3.05^{de}
F3	34.33 ± 1.50^{ijk}	28.33 ± 2.95^{ghi}	37.32 ± 0.46^{gh}
F4	20.97 ± 1.24^{mn}	29.65 ± 3.31^{hi}	49.39 ± 1.82^{k}
Q1	52.19 ± 1.72^{bcde}	24.04 ± 2.25^{de}	23.77 ± 2.12^{cd}
Q2	42.23 ± 0.80^{fghi}	23.94 ± 1.88^{de}	33.83 ± 1.11^{fg}
Q3	34.11 ± 1.01^{ijk}	21.98 ± 0.41^{cd}	43.89 ± 1.31^{j}
Q4	22.00 ± 0.25^{lmn}	23.32 ± 0.85^{cde}	54.68 ± 1.10^{l}
GA1	48.25 ± 1.82^{cdef}	28.5 ± 4.56^{ghi}	23.25 ± 4.56^{cd}
GA2	36.5 ± 2.12^{hijk}	29.25 ± 4.22^{hi}	34.25 ± 4.22^{gh}
GA3	30.25 ± 1.10^{klm}	30.5 ± 3.34^{i}	39.25 ± 1.10^{hi}
GA4	20.50 ± 3.05^{n}	35.75 ± 3.98^{j}	43.75 ± 3.05^{j}
RT1	60.25 ± 3.87^{b}	14.50 ± 3.87^{a}	25.25 ± 3.87^{de}
RT2	55.50 ± 3.34^{bcd}	14.50 ± 3.34^{a}	30.00 ± 3.34^{ef}
RT3	45.25 ± 3.12^{efgh}	20.25 ± 3.12^{bc}	34.50 ± 3.12^{gh}
RT4	30.50 ± 2.56^{kl}	27.25 ± 2.56^{fgh}	42.25 ± 2.56^{ij}
CT1	56.25 ± 4.56^{bc}	24.25 ± 5.56^{def}	19.50 ± 5.56^{b}
CT2	50.50 ± 4.22^{cdef}	24.50 ± 4.98^{def}	25.00 ± 4.98^{de}
CT3	40.25 ± 3.34^{ghij}	29.75 ± 4.34^{hi}	30.00 ± 3.34^{fg}
CT4	30.50 ± 3.98^{kl}	29.44 ± 4.56^{hi}	40.06 ± 3.98^{ij}
ES1	61.25 ± 4.56^{b}	21.25 ± 2.77^{cd}	17.50 ± 2.77^{b}
ES2	56.5 ± 4.22^{bc}	18.50 ± 3.23^{b}	25.00 ± 3.23^{cd}
ES3	46.25 ± 3.12^{defg}	22.75 ± 2.98^{cd}	31.00 ± 3.12^{fg}
ES4	31.502 ± 2.56^{jk}	28.50 ± 3.12^{ghi}	40.00 ± 2.56^{ij}
Values are mean of triplicates ±SD; Values with different letters in the same column differ significantly ($p<0.05$)			

4.3.2.2 Predicted glycemic index (pGI)

In vitro digestion analyses demonstrated that polyphenols could successfully retard starch digestibility. To further comprehend the enzymatic hydrolysis of the complexes, the rate of starch digestion against digestion time of all the samples were calculated. The starch hydrolysis pattern of the different starch-polyphenols complexes was plotted and presented (Fig. 4.14). The starch hydrolysis pattern of EFKS-ferulic acid complex is displayed [Fig 4.14 (a)], the starch hydrolysis pattern of EFKS-quercetin complex is displayed in Fig 4.14 (b), the starch digestion pattern of EFKS-gallic acid complex is presented [Fig 4.14 (c)], the starch hydrolysis pattern of EFKS-rutin complex is presented [Fig 4.14 (d)], the starch hydrolysis pattern of EFKS-catechin complex is presented [Fig 4.14 (e)], and the starch hydrolysis pattern of EFKS- *Euryale ferox* seed shell extract complex is presented [Fig 4.14 (f)].

The pGI (predicted glycemic index) were determined from starch digestion curves using the equation of Goni et al. (1997) [12]. The decrease in starch hydrolysis rate, which is proportional to the concentration of polyphenols. The first order kinetics was applied to determine the reaction rate constant 'k'. The 'k' of the control pregelatinized *Euryale ferox* kernel starch was 0.0913. The rate constant 'k' value declined as the concentrations of the polyphenols raised (Table 4.2). For the gelatinized *Euryale ferox* kernel starch, the equilibrium concentration (C∞), or the amount of hydrolysis at which the hydrolysis curve reached a plateau, was 92.31%. Whereas, C∞ of the developed complexes were in the range of 82.50 % (ES4) to 45.32 (Q4). Both the C∞ and k trends were in perfect agreement with one another. Thus, we can conclude that the concentration of polyphenols added in the present study were indeed effective in inhibiting the *in vitro* starch hydrolysis. The hydrolysis index (HI) of the complexes was in the range of 84.62 (F1) and 41.91% (GA4). It was found that pregelatinized *Euryale ferox* kernel starch (PS) had the highest pGI value (96.56) and the pGI of the starch-polyphenols complexes were in the range between 86.17 (F1) to 62.72 (GA4) (Table 4.2). Although the SDS and RS fractions of the complexes containing 2.5 to 7.5% polyphenols were significantly increased, the pGI of the complexes still falls under high GI. However, complexes containing 10% phenolic compounds falls under intermediate GI such as F4 (64.71), Q4 (63.37), GA4 (62.72), CT4 (64.45) and ES4 (66.20). The finding of the present study proved that starch-polyphenols interactions inhibit digestibility and reduce the GI of carbohydrate rich foods. These complexes having high RS and low GI starch may be incorporated in functional foods to solve the ever-increasing problem of obesity and diabetes.

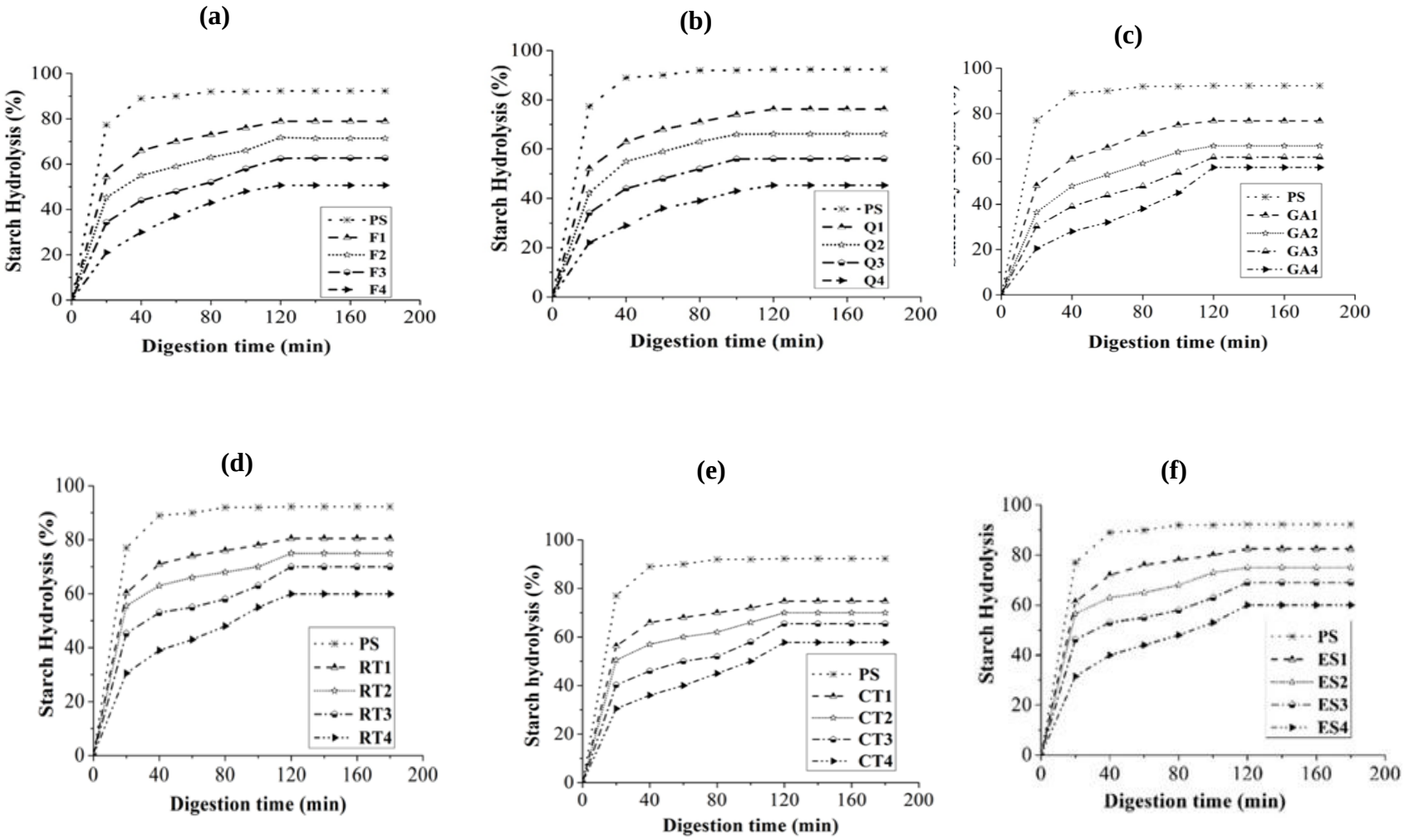

Fig. 4.14 (a) Starch hydrolysis kinetics of *Euryale ferox* kernel starch-ferulic acid complex; **(b)** *Euryale ferox* kernel starch-quercetin complex **(c)** *Euryale ferox* kernel starch-gallic acid complex; **(d)** *Euryale ferox* kernel starch-rutin complex **(e)** *Euryale ferox* kernel starch-catechin complex **(f)** *Euryale ferox* kernel starch-*Euryale ferox* seed shell extract complex

Table 4.2 Determination of predicted glycemic index (pGI) of the *Euryale ferox* kernel starch-polyphenols complex

Sample	**∞ (%)**	**k value (min)**	**HI (%)**	**Predicted GI**
PS	92.31±4.00^{a}	0.09132±0.004^{a}	103.56±4.82^{a}	96.56±2.65^{a}
F1	78.93±2.94^{b}	0.05426±0.000^{b}	84.62±3.15^{b}	86.17±1.73^{b}
F2	71.56±2.41^{ef}	0.04287±0.002^{c}	74.60±3.04^{c}	80.66±1.67^{c}
F3	62.50±1.93^{hij}	0.03104±0.001^{d}	61.62±2.68^{ef}	73.37±1.47^{ef}
F4	50.62±1.82^{mn}	0.02232±0.002^{g}	45.54±0.16^{i}	64.71±0.08^{i}
Q1	76.23±2.12^{bcd}	0.05284±0.003^{c}	81.44±1.82^{b}	84.42±0.99^{b}
Q2	66.17±1.11^{gh}	0.04747±0.002^{d}	69.76±0.61^{cd}	78.01±0.33^{cd}
Q3	56.10±1.30^{jk}	0.04156±0.000^{g}	58.06±1.39^{g}	71.59±0.76^{g}
Q4	45.32±1.12^{n}	0.02700±0.001^{i}	43.09±1.43^{i}	63.37±0.78^{i}
GA1	76.75±2.36^{cde}	0.04284±0.005^{j}	79.79±2.09^{cd}	83.51±1.14^{cd}
GA2	65.75±2.12^{ij}	0.03403±0.003^{l}	65.74±2.01^{gh}	75.80±1.10^{gh}
GA3	60.75±1.76^{kl}	0.02465±0.001^{q}	56.40±2.17^{i}	70.67±1.19^{i}
GA4	56.25±1.55^{lm}	0.01345±0.001^{r}	41.91±1.56^{k}	62.72±0.85^{k}
RT1	74.58±0.52^{def}	0.06734±0.006^{e}	81.74±0.61^{cd}	84.58±0.33^{cd}
RT2	70.83±1.04^{fgh}	0.06361±0.005^{f}	77.22±1.16^{de}	82.10±0.63^{de}
RT3	65.83±1.04^{ij}	0.05242±0.003^{h}	70.30±1.19^{fg}	78.30±0.65^{fg}
RT4	57.92±1.01^{klm}	0.03062±0.002^{k}	56.68±1.18^{i}	70.82±0.64^{i}
CT1	80.83±1.04^{bc}	0.01727±0.001^{o}	66.88±1.20^{gh}	76.43±0.66^{gh}
CT2	75.50±1.32^{def}	0.01714±0.001^{o}	62.30±1.29^{h}	73.91±0.70^{h}
CT3	71.32±1.52^{fg}	0.01620±0.001^{p}	57.57±1.56^{i}	71.32±0.85^{i}
CT4	60.65±1.17^{kl}	0.01337±0.001^{r}	45.06±1.24^{jk}	64.45±0.68^{jk}
ES1	82.50±2.22^{b}	0.01857±0.001^{m}	70.11±2.32^{fg}	78.20±1.27^{fg}
ES2	75.00±1.56^{def}	0.01844±0.003^{mn}	63.57±2.13^{h}	74.61±1.72^{h}
ES3	69.00±1.89^{ghi}	0.01758±0.002^{no}	57.47±2.23^{i}	71.26±1.22^{i}
ES4	62.60±2.94^{jk}	0.01452±0.001^{p}	48.26±2.28^{j}	66.20±1.25^{j}
Values are mean of triplicates ±SD; Values with the different letters in the same column differ significantly ($p<0.05$)				

4.3.3 Antioxidant activity

The scavenging abilities of EFKS-polyphenol complex against DPPH radicals were assessed. Starch has negligible reducing power because the strong intramolecular and intermolecular hydrogen bonds interactions between the hydroxyl groups in the starch molecules limit the hydrogen donating capacity [45]. Whereas all EFKS-polyphenols exhibited free radicals scavenging capacity. As shown in Fig. 4.15, the DPPH radical scavenging activities of EFKS-polyphenol complex (62.30–66.34%). The highest DPPH free-radical scavenging capability was found in the Q4 sample, while the lowest was exhibited by the Q1. A dose-dependent surge in free radical scavenging capacity was observed. The contribution of the phenolic hydroxyl groups bound to the starch must be responsible for rendering antioxidant properties of the prepared complexes. Higher degree of complexation had a higher level of scavenging. The ability of the polyphenol moieties to transfer electrons and donate hydrogen atoms might be accountable for the increased free radical scavenging activity of the complexes. The key structural element responsible for catechin's antioxidant action is the hydroxyl group located at position 3-C. Catechin bound to the starch with hydroxyl groups that might neutralize free radicals, terminating free radical chain reactions [39].

From the ^{1}H NMR spectra, it observed that, a small portion of OH was deployed in the complexation process, thus a large portion of OH were left unbound in the complexes and thus exhibited its significant antioxidant activity [25]. As a result of these findings, it appears that complexation could successfully load polyphenols onto starch and enhance the antioxidant properties of starch. Likewise, some researchers reported that the complexation of the polyphenol with the polysaccharide improved its capacity to scavenge DPPH radicals [26, 39]. So, nutraceutical business may explore into this new class of modified starch called starch-polyphenols complex, which is low in glycemic index and rich in antioxidants [45].

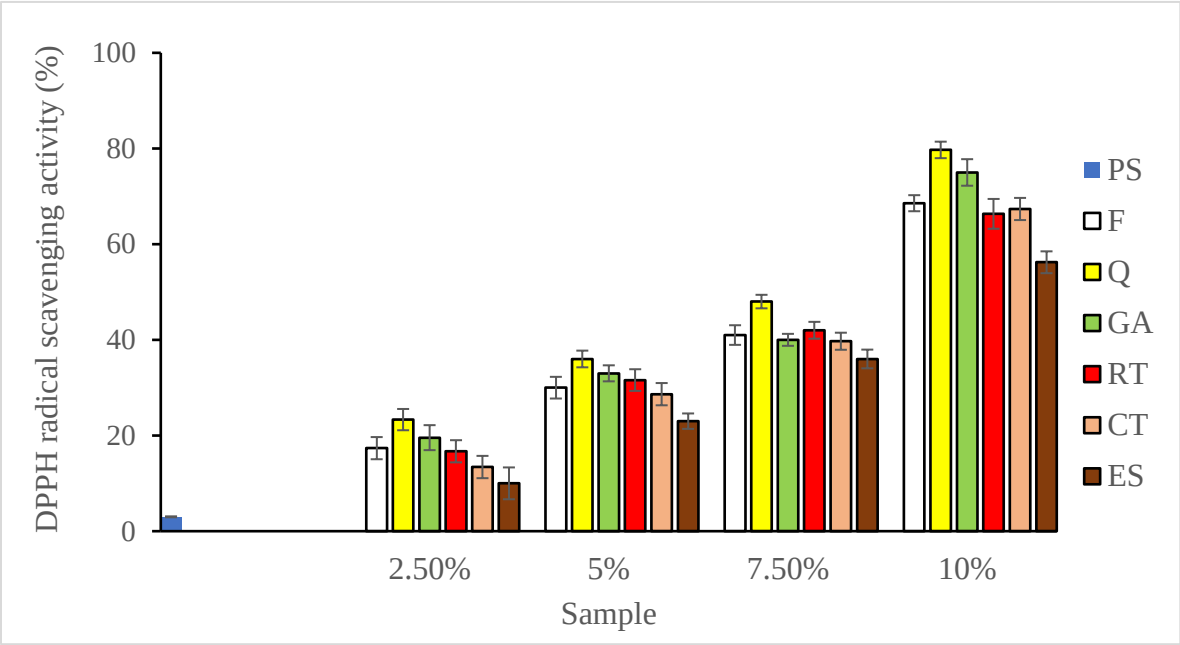

Fig. 4.15 DPPH radical scavenging activity of *Euryale ferox* kernel starch-polyphenols complex

4.3.4 Color characteristics

Color characteristics (L*, a*, and b*) of the complexes were measured and displayed in Table 4.3. Compared to the control, ferulic acid and quercetin addition decreased L* values significantly in all the prepared complex. Addition of ferulic acid up to 5% did not impart significant changes to the complex with respect to its a* and b* values. Quercetin complexation produced lower L* values complexes as compared to the control. The *Euryale ferox* kernel starch-quercetin, and starch-rutin complexes were yellowish in color, as demonstrated by significant increase in b* values. Whereas, the *Euryale ferox* kernel starch-catechin, and starch-EFSSE complexes were reddish in color, as demonstrated by significant increase in a* values. The bathochromic shift of the catechin, quercetin and rutin contained in the sample may be accountable for the dramatic changes. This demonstrated that the final color of the complexes is determined by the color of the polyphenols used for complexation.

Table 4.3 Color properties of *Euryale ferox* kernel starch-polyphenols complex

Sample	L*	a*	b*
PS	98.66±0.01^{a}	0.19±0.02^{c}	4.07±0.02^{a}
F1	90.68±0.37^{b}	0.10±0.01^{c}	5.81±0.17^{ab}
F2	89.63±0.47^{b}	0.18±0.04^{c}	7.07±1.75^{ab}
F3	88.31±0.24^{b}	0.20±0.00^{c}	7.26±0.08^{ab}
F4	88.02±1.59^{b}	0.29±0.09^{c}	8.09±0.92^{b}
Q1	65.93±1.32^{e}	-1.10±0.03^{b}	42.48±0.61^{h}
Q2	71.61±0.24^{d}	-7.08±0.00^{a}	42.52±0.64^{h}
Q3	73.97±2.62^{cd}	-3.94±0.18^{b}	43.50±0.93^{h}
Q4	75.97±0.73^{c}	-2.65±0.59^{b}	44.38±0.25^{h}
GA1	89.77^{b}	0.01^{c}	5.85^{ab}
GA2	89.15^{b}	0.01^{c}	6.27^{ab}
GA3	88.34^{b}	0.02^{c}	7.24^{ab}
GA4	86.42^{b}	0.07^{c}	7.79^{ab}
RT1	48.40^{i}	-4.29^{a}	20.62^{e}
RT2	54.54^{gh}	-4.73^{a}	20.97^{e}
RT3	61.34^{f}	-6.12^{a}	25.14^{f}
RT4	67.81^{e}	-7.57^{a}	35.07^{g}
CT1	60.90^{f}	2.08^{d}	10.95^{c}
CT2	59.75^{fg}	2.7^{d}	10.82^{c}
CT3	57.65^{fg}	2.24^{d}	8.47^{bc}
CT4	56.54^{gh}	2.16^{d}	7.67^{b}
ES1	72.49^{d}	2.16^{d}	13.31^{cd}
ES2	61.90^{f}	2.68^{d}	13.53^{cd}
ES3	62.27^{f}	2.78^{d}	13.88^{cd}
ES4	59.50^{fg}	3.22^{de}	14.18^{cd}
Values are mean of triplicates ±SD; Values with the different letters in the same column differ significantly ($p<0.05$)			

4.3.5 Swelling power and solubility index

Solubility and swelling power indicate the capability of starch granules to dissolve and expand during the gelatinization process. It is determined by the degree of interaction between the crystalline and amorphous regions of starch granules [3]. It was observed that the swelling power of pregelatinized *Euryale ferox* kernel starch was lesser as compared to the native starch, in the range of 9.57 -12.05 g/g. It is because hydrothermal treatment ruptured starch chains, thus inhibiting the swelling of starch granules [10]. The impact of polyphenols inclusion on the swelling capacity and solubility index of starch is presented in Table 4.4. There was a concentration dependent decrease in the swelling power in all of the complexes. Among all the complexes, F1 (2.5% ferulic acid) exhibited least reduction 16.20 (g/g) while GA4 (10 % gallic acid) exhibited least swelling capacity of 6.86 g/g.

Our findings are in agreement with a prior study which reported that complexation of potato starch with ferulic acid and gallic acid could lower the swelling capacity of the starch significantly [19]. In the similar pattern, the addition of quercetin reduced the swelling power of pregelatinized *Euryale ferox* kernel starch. The declining trend became more evident as polyphenols addition increased in all of the complexes. Addition of polyphenols rendered a more organized and tighter crystal structure as observed in XRD pattern, and amylose leaching was inhibited, thus reducing gelatinization, and swelling power. It was postulated that during complexation, polyphenols that diffuse in water could modify the water activity and ionic stability of the solution and compete with starch granules for hydration, leading to reduced swelling capacity [17].

The solubility index of the pregelatinized *Euryale ferox* kernel starch was 8.31 %, as compared to 2.5-3% for native starch whereas 15.03 % and 3.22 % for solutions containing 10% ferulic acid and 2.5 % catechin respectively. Increased water solubility of starch-ferulic acid complexes occurred due to improve starch-water interactions [16]. However, the reduced solubility of starch-polyphenols complex occurred due to the low water solubility of quercetin, which greatly hinders the starch-water interaction [16, 29]. Thus, the impact of polyphenols complexation on starch largely depends on the solubility of the added compound in the reaction medium.

Table 4.4 Swelling power and solubility of *Euryale ferox* kernel starch-polyphenols complex

Sample	Swelling power (g/g)	Solubility index (%)
PS	19.60 ± 0.60^{a}	8.31 ± 0.75^{c}
F1	16.20 ± 0.72^{b}	15.03 ± 1.17^{a}
F2	14.87 ± 1.00^{bc}	12.06 ± 0.76^{a}
F3	12.05 ± 0.91^{c}	11.36 ± 0.24^{a}
F4	10.52 ± 1.30^{cd}	10.55 ± 0.65^{bc}
Q1	18.81 ± 0.31^{a}	7.28 ± 0.29^{cd}
Q2	16.49 ± 0.43^{ab}	6.76 ± 0.57^{cd}
Q3	14.46 ± 0.44^{bc}	5.41 ± 0.48^{cd}
Q4	11.36 ± 0.55^{cd}	4.66 ± 0.288^{de}
GA1	8.40 ± 0.61^{d}	3.40 ± 0.51^{de}
GA2	7.90 ± 0.94^{d}	3.71 ± 0.22^{de}
GA3	7.41 ± 0.61^{d}	4.22 ± 0.54^{de}
GA4	6.86 ± 0.50^{d}	4.52 ± 0.25^{de}
RT1	8.37 ± 0.65^{d}	3.44 ± 0.47^{cde}
RT2	7.99 ± 0.98^{d}	4.05 ± 0.11^{abcde}
RT3	7.46 ± 0.68^{d}	4.54 ± 0.51^{cde}
RT4	7.06 ± 0.05^{d}	4.74 ± 0.99^{cde}
CT1	8.48 ± 0.50^{d}	3.22 ± 0.22^{e}
CT2	8.16 ± 0.90^{d}	4.36 ± 0.46^{cde}
CT3	7.82 ± 0.77^{d}	4.47 ± 0.22^{cde}
CT4	7.28 ± 0.80^{d}	4.57 ± 0.16^{cde}
ES1	17.46 ± 0.98^{ab}	8.55 ± 0.40^{c}
ES2	14.48 ± 0.72^{bc}	7.5 ± 0.32^{cd}
ES3	10.55 ± 0.50^{cd}	6.4 ± 0.22^{cd}
ES4	9.15 ± 0.44^{cd}	4.43 ± 0.36^{cde}
Values are mean of triplicates ±SD; Values with the different letters in the same column differ significantly ($p<0.05$)		

4.4 Conclusion

The result obtained from XRD and FTIR, NMR, and DSC confirms the complexation of starch and polyphenols. The morphology of EFKS became more compact and smoother with the addition of polyphenols. The addition of polyphenols could change the color, lowering the swelling capacity. Complexation of *Euryale ferox* kernel starch with polyphenols could modulating the digestibility and thus lowered the glycemic index. The structural modification of the starch may be accountable for the observed effect. Therefore, starch-polyphenol complex may be considered a potential raw material for manufacturing functional foods and nutraceuticals. The findings of this study will also help to fully understand the changes that might occur when *Euryale ferox* seed is boiled along with its shells and promote the process of cooking along with its shell before being processed or eating.

Bibliography

1. Amoako, D. B., & Awika, J. M. Polymeric tannins significantly alter properties and *in vitro* digestibility of partially gelatinized intact starch granule. *Food Chemistry*, 208: 10-17, 2016
2. Božič, M., Gorgieva, S., & Kokol, V. Laccase-mediated functionalization of chitosan by caffeic and gallic acids for modulating antioxidant and antimicrobial properties. *Carbohydrate Polymers*, 87(4): 2388-2398, 2012.
3. Chen, N., Gao, H. X., He, Q., Yu, Z. L., & Zeng, W. C. Interaction and action mechanism of starch with different phenolic compounds. *International Journal of Food Sciences and Nutrition*, 71(6): 726-737, 2020.
4. Chi, C., Li, X., Zhang, Y., Chen, L., Xie, F., Li, L., & Bai, G. Modulating the *in vitro* digestibility and predicted glycemic index of rice starch gels by complexation with gallic acid. *Food Hydrocolloids*, 89, 821-828, 2019.
5. Chi, Chengdeng, Xiaoxi Li, Yiping Zhang, Ling Chen, Lin Li, and Zhijiang Wang. "Digestibility and supramolecular structural changes of maize starch by non-covalent interactions with gallic acid." *Food and Function*, 8(2): 720-730, 2017.
6. Chumsri, P., Panpipat, W., Cheong, L. Z., Nisoa, M., & Chaijan, M. Comparative Evaluation of Hydrothermally Produced Rice Starch–Phenolic Complexes:

Contributions of Phenolic Type, Plasma-Activated Water, and Ultrasonication. *Foods*, 11(23): 3826, 2022.

7. Deng, N., Deng, Z., Tang, C., Liu, C., Luo, S., Chen, T., & Hu, X. Formation, structure and properties of the starch-polyphenol inclusion complex: A review. *Trends in Food Science and Technology*, 112: 667-675, 2021.
8. Englyst, H. N., Kingman, S. M., & Cummings, J. H. Classification and measurement of nutritionally important starch fractions. *European Journal of Clinical Nutrition*, 46: S33-50, 1992.
9. Fang, K., He, W., Jiang, Y., Li, K., & Li, J. Preparation, characterization and physicochemical properties of cassava starch-ferulic acid complexes by mechanical activation. *International Journal of Biological Macromolecules*, 160:482-488, 2020.
10. Gao, S., Liu, H., Sun, L., Cao, J., Yang, J., Lu, M., & Wang, M. (2021). Rheological, thermal and *in vitro* digestibility properties on complex of plasma modified Tartary buckwheat starches with quercetin. *Food Hydrocolloids*, 110: 106209, 2021.
11. Giuberti, G., Rocchetti, G., & Lucini, L. Interactions between phenolic compounds, amylolytic enzymes and starch: An updated overview. *Current Opinion in Food Science*, 31:102-113, 2020
12. Goni, I., Garcia-Alonso, A., & Saura-Calixto, F. A starch hydrolysis procedure to estimate glycemic index. *Nutrition Research*, 17(3): 427-437, 1997.
13. Gutierrez, A. S. A., Guo, J., Feng, J., Tan, L., & Kong, L. Inhibition of starch digestion by gallic acid and alkyl gallates. *Food Hydrocolloids*, *102*, 105603, 2020
14. Han, X., Zhang, M., Zhang, R., Huang, L., Jia, X., Huang, F., & Liu, L. Physicochemical interactions between rice starch and different polyphenols and structural characterization of their complexes. *LWT- Food Science and Technology*, 125: 109227, 2020.
15. Igoumenidis, P. E., Zoumpoulakis, P., & Karathanos, V. T. (2018). Physicochemical interactions between rice starch and caffeic acid during boiling. *Food Research International*, 109: 589-595, 2018.
16. Karunaratne, R., & Zhu, F. Physicochemical interactions of maize starch with ferulic acid. *Food Chemistry*, 199: 372-379, 2016.

17. Li, H., Zhai, F., Li, J., Zhu, X., Guo, Y., Zhao, B., & Xu, B. Physicochemical properties and structure of modified potato starch granules and their complex with tea polyphenols. *International Journal of Biological Macromolecules*, 166: 521-528, 2021.
18. Li, L., Liu, Y., Xue, Y., Zhu, J., Wang, X., & Dong, Y. Preparation of a ferulic acid–phospholipid complex to improve solubility, dissolution, and B16F10 cellular melanogenesis inhibition activity. *Chemistry Central Journal*, 11: 1-8, 2017.
19. Li, M., Ndiaye, C., Corbin, S., Foegeding, E. A., & Ferruzzi, M. G. Starch-phenolic complexes are built on physical CH-π interactions and can persist after hydrothermal treatments altering hydrodynamic radius and digestibility of model starch-based foods. *Food Chemistry*, 308: 125577, 2020.
20. Li, Y., Gao, S., Ji, X., Liu, H., Liu, N., Yang, J., Lu, M., Han, L., & Wang, M. Evaluation studies on effects of quercetin with different concentrations on the physicochemical properties and *in vitro* digestibility of Tartary buckwheat starch. *International Journal of Biological Macromolecules*, 163:1729-1737, 2020.
21. Li., Wang, L., Wang, T., Li, Z., Gao, Y., Cui, S. W., & Qiu, J. Comparison of quercetin and rutin inhibitory influence on Tartary buckwheat starch digestion *in vitro* and their differences in binding sites with the digestive enzyme. *Food Chemistry*, 367: 130762, 2022.
22. Liu, B., Zhong, F., Yokoyama, W., Huang, D., Zhu, S., & Li, Y. Interactions in starch co-gelatinized with phenolic compound systems: Effect of complexity of phenolic compounds and amylose content of starch. *Carbohydrate Polymers*, 247, 116667, 2020.
23. Liu, J., Wen, X. Y., Lu, J. F., Kan, J., & Jin, C. H. Free radical mediated grafting of chitosan with caffeic and ferulic acids: Structures and antioxidant activity. *International Journal of Biological Macromolecules*, 65: 97-106, 2014.
24. Liu, Y., Chen, L., Xu, H., Liang, Y., & Zheng, B. Understanding the digestibility of rice starch-gallic acid complexes formed by high pressure homogenization. *International Journal of Biological Macromolecules*, 134: 856-863, 2019.

25. Liu, Y., Wei, S., & Liao, M. Optimization of ultrasonic extraction of phenolic compounds from *Euryale ferox* seed shells using response surface methodology. *Industrial Crops and Products,* 49: 837-843, 2013.

26. Lv, X., Ye, F., Li, J., Ming, J., & Zhao, G. Synthesis and characterization of a novel antioxidant RS4 by esterifying carboxymethyl sweetpotato starch with quercetin. *Carbohydrate Polymers*, *152*: 317-326, 2016.

27. Mathew, S., & Abraham, T. E. Physico-chemical characterization of starch ferulates of different degrees of substitution. *Food Chemistry*, 105(2): 579-589, 2007.

28. Nguyen, T. A., Liu, B., Zhao, J., Thomas, D. S., & Hook, J. M. An investigation into the supramolecular structure, solubility, stability and antioxidant activity of rutin/cyclodextrin inclusion complex. *Food Chemistry*, 136(1): 186-192, 2013.

29. Ren, N., Ma, Z., Li, X., & Hu, X. Preparation of rutin-loaded microparticles by debranched lentil starch-based wall materials: Structure, morphology and in vitro release behavior. *International Journal of Biological Macromolecules*, 173: 293-306, 2021.

30. Shi, L., Zhou, J., Guo, J., Gladden, I., & Kong, L. Starch inclusion complex for the encapsulation and controlled release of bioactive guest compounds. *Carbohydrate Polymers*, 274: 118596, 2021.

31. Singh, A., Dutta, P. K., Kumar, H., Kureel, A. K., & Rai, A. K. Synthesis of chitin-glucan-aldehyde-quercetin conjugate and evaluation of anticancer and antioxidant activities. *Carbohydrate Polymers*, 193: 99-107, 2018.

32. Song, C. W., Wang, S. M., Zhou, L. L., Hou, F. F., Wang, K. J., Han, Q. B., Li, N., & Cheng, Y. X. Isolation and identification of compounds responsible for antioxidant capacity of *Euryale ferox* seeds. *Journal of Agricultural and Food Chemistry*, 59(4): 1199-1204, 2011.

33. Sun, L., & Miao, M. Dietary polyphenols modulate starch digestion and glycaemic level: A review. *Critical Reviews in Food Science and Nutrition*, 60(4): 541-555, 2020.

34. Wang, L., Wang, L., Li, Z., Gao, Y., Cui, S. W., Wang, T., & Qiu, J. Diverse effects of rutin and quercetin on the pasting, rheological and structural properties of Tartary buckwheat starch. *Food Chemistry*, 335: 127556, 2021.
35. Wang, L., Wang, L., Wang, T., Li, Z., Gao, Y., Cui, S. W., & Qiu, J. Comparison of quercetin and rutin inhibitory influence on Tartary buckwheat starch digestion *in vitro* and their differences in binding sites with the digestive enzyme. *Food Chemistry*, 367: 130762, 2022.
36. Wang, M., Shen, Q., Hu, L., Hu, Y., Ye, X., Liu, D., & Chen, J. Physicochemical properties, structure and *in vitro* digestibility on complex of starch with lotus (Nelumbo nucifera Gaertn.) leaf flavonoids. *Food Hydrocolloids*, 81: 191-199, 2018.
37. Wen, Y., Ye, F., Zhu, J., & Zhao, G. Corn starch ferulates with antioxidant properties prepared by N, N′-carbonyldiimidazole-mediated grafting procedure. *Food Chemistry*, 208: 1-9, 2016.
38. Xu, T., Li, X., Ji, S., Zhong, Y., Simal-Gandara, J., Capanoglu, E., Xiao, J., & Lu, B. Starch modification with phenolics: Methods, physicochemical property alteration, and mechanisms of glycemic control. *Trends in Food Science and Technology*, 111: 12-26, 2021.
39. Yong, H., Bai, R., Bi, F., Liu, J., Qin, Y., & Liu, J. Synthesis, characterization, antioxidant and antimicrobial activities of starch aldehyde-quercetin conjugate. *International Journal of Biological Macromolecules*, 156: 462-470, 2020.
40. Yu, J. Y., Roh, S. H., & Park, H. J. Characterization of ferulic acid encapsulation complexes with maltodextrin and hydroxypropyl methylcellulose. *Food Hydrocolloids*, 111: 106390, 2021.
41. Yu, M., Liu, B., Zhong, F., Wan, Q., Zhu, S., Huang, D., & Li, Y. Interactions between caffeic acid and corn starch with varying amylose content and their effects on starch digestion. *Food Hydrocolloids*, 114: 106544, 2021.
42. Zhang, L., Yang, X., Li, S., & Gao, W. Preparation, physicochemical characterization and *in vitro* digestibility on solid complex of maize starches with quercetin. *LWT-Food Science and Technology*, 44(3):787-792, 2011.
43. Zhao, B., Wang, B., Zheng, B., Chen, L., & Guo, Z. Effects and mechanism of high-pressure homogenization on the characterization and digestion behavior of lotus seed

starch–green tea polyphenol complexes. *Journal of Functional Foods*, 57: 173-181, 2019.

44. Zheng, Y., Tian, J., Kong, X., Yang, W., Yin, X., Xu, E., Chen, S., Liu, D., & Ye, X. Physicochemical and digestibility characterization of maize starch–caffeic acid complexes. *LWT- Food Science and Technology*, 121: 108857, 2020.
45. Zhou, Y., Jiang, Q., Ma, S., & Zhou, X. Effect of quercetin on the *in vitro* Tartary buckwheat starch digestibility. *International Journal of Biological Macromolecules*, 183: 818-830, 2021.
46. Zhu, W., & Zhang, Z. Preparation and characterization of catechin-grafted chitosan with antioxidant and antidiabetic potential. *International Journal of Biological Macromolecules*, 70: 150-155, 2014.